






Review

Switched Reluctance Motors and Drive Systems for Electric Vehicle Powertrains: State of the Art Analysis and Future Trends

Yuanfeng Lan ^{1,2}, Yassine Benomar ^{1,2}, Kritika Deepak ^{1,2}, Ahmet Aksoz ^{1,2}, Mohamed El Baghdadi ^{1,2}, Emine Bostanci ³ and Omar Hegazy ^{1,2,*}

¹ ETEC Department & MOBI Research Centre, Vrije Universiteit Brussel (VUB), Pleinlaan 2, 1050 Brussels, Belgium; yuanfeng.lan@vub.be (Y.L.); yassine.benomar@vub.be (Y.B.); kritika.deepak@vub.be (K.D.); ahmet.aksoz@vub.be (A.A.); mohamed.el.baghdadi@vub.be (M.E.B.)

² Flanders Make, 3001 Heverlee, Belgium

³ Electrical and Electronics Engineering Department, Middle East Technical University, 06800 Ankara, Turkey; emineb@metu.edu.tr

* Correspondence: omar.hegazy@vub.be; Tel.: +32-2-629-2992

Abstract: This paper presents a detailed literature review on switched reluctance motor (SRM) and drive systems in electric vehicle (EV) powertrains. SRMs have received increasing attention for EV applications owing to their reliable structure, fault tolerance ability and magnet free design. The main drawbacks of the SRM are torque ripple, low power density, low power factor and small extended speed range. Recent research shows that multi-stack conventional switched reluctance motors (MSCSRM) and multi-stack switched reluctance motors with a segmental rotor (MSSRM-SR) are promising alternative solutions to reduce torque ripples, increase torque density and increase power factor. Different winding configurations such as single-layer concentrated winding (SLC), single layer mutually coupled winding (SLMC), double layer concentrated winding (DLC), double layer mutually coupled winding (DLMC) and fully-pitched winding (FP) are introduced in the literature in recent years to increase average torque and to decrease torque ripples. This research analyzes winding methods and structure of the SRMs, including conventional and segmental rotors. They have been compared and assessed in detail evaluation of torque ripple reduction, torque/power density increase, noise/vibration characteristics and mechanical structure. In addition, various drive systems are fully addressed for the SRMs, including conventional drives, soft-switching drives, drives with standard inverters and drives with an integrated battery charger. In this paper, the SRM control methods are also reviewed and classified. These control methods include strategies of torque ripple reduction, fault-diagnosis, fault-tolerance techniques and sensorless control. The key contributions of this paper provide a useful basis for detailed analysis of modeling and electromechanical design, drive systems, and control techniques of the SRMs for EV applications.

Keywords: switched reluctance motor; segSRM; multi-stack; SRM converter; speed control; torque ripple reduction



Citation: Lan, Y.; Benomar, Y.; Deepak, K.; Aksoz, A.; Baghdadi, M.E.; Bostanci, E.; Hegazy, O. Switched Reluctance Motors and Drive Systems for Electric Vehicle Powertrains: State of the Art Analysis and Future Trends. *Energies* **2021**, *14*, 2079. <https://doi.org/10.3390/en14082079>

Academic Editor: Aldo Sornioti

Received: 3 March 2021

Accepted: 29 March 2021

Published: 8 April 2021

Publisher's Note: MDPI stays neutral with regard to jurisdictional claims in published maps and institutional affiliations.



Copyright: © 2021 by the authors. Licensee MDPI, Basel, Switzerland. This article is an open access article distributed under the terms and conditions of the Creative Commons Attribution (CC BY) license (<https://creativecommons.org/licenses/by/4.0/>).

1. Introduction

The switched reluctance motor (SRM) has some advantages compared to the induction motor (IM) and permanent magnet synchronous motor (PMSM), such as a magnet-free and robust rotor structure that allows high speed operations and is inherently fault tolerant. Due to these reasons, SRM is a promising traction machine candidate for electric vehicle (EV) applications. The SRM can be driven by an asymmetric bridge, thus avoiding the risk of short-circuits across the dc source. The main disadvantages of the SRM are its high torque ripple [1], low torque/power density and low power factor [2,3].

Torque ripple minimization is one of the most important and challenging SRM design aspects when the requirements of traction applications are considered. Two approaches are

used to decrease torque ripples: structural design and advanced SRM control methods [4]. Furthermore, multi-stack and multi-layer structures were introduced to further reduce the torque ripples of the SRMs [5–8]. Different converter topologies and control methods were developed to decrease the torque ripples [4].

In this paper, the conventional and the segmental SRM designs, drive topologies and control methods of the SRMs for higher average torque with less torque ripples, less vibration, and less acoustic noises in the EVs are discussed. In Section 2, the conventional SRM structure is analyzed, and winding configuration classifications are described. Then, a review of one-stack and multi-stack conventional SRMs is presented. Section 3 introduces the segSRM, including the one-stack and the multi-stack segmental SRM. In Section 4, different drives for the SRMs are classified, and a summary of conventional converters for the SRMs is provided. Furthermore, soft-switching converters for the SRMs are reviewed. The SRM drives with standard voltage source inverters (VSIs) are also presented. This section is concluded with an investigation on the SRM drives integrated with the EV battery chargers. Section 5 presents the control methods of SRMs, including control methods for torque ripple reduction, fault-diagnosis, fault-tolerance techniques and sensorless control for the SRMs. Finally, a conclusion and future trends are given in Section 6.

2. Conventional Switched Reluctance Motor

A conventional SRM (CSRSM) consists of three parts, which are winding, stator and rotor. The most common conventional SRMs with different stator and rotor pole ratios are shown in Figure 1 [9]. The tendency of the magnetic flux to have a minimum reluctance is what produces the electromagnetic torque in the SRM. Once the rotor pole is aligned to the stator pole, the maximum inductance of the excited phase is obtained.

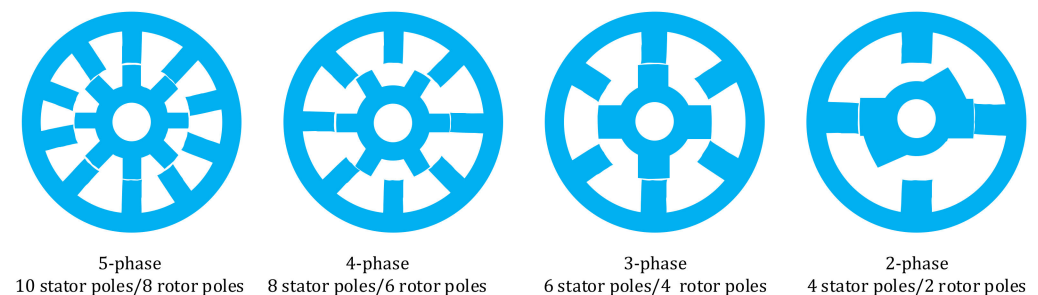


Figure 1. Conventional SRMs with different numbers of stator and rotor poles [9].

The instantaneous voltage between the terminals of a single phase can be expressed as Equation (1) [9]:

$$U = iR + d\varnothing/dt, \quad (1)$$

where U is the instantaneous voltage on each phase, i is the phase current, R is the resistance of a phase, \varnothing is the flux linkage, and t is the time. The flux linkage changes with the rotor position and phase current value:

$$U = iR + \partial\varnothing/\partial I \times di/dt + \partial\varnothing/\partial\theta \times d\theta/dt = iR + L(\theta,i) \times di/dt + E(\theta,i) \times d\theta/dt, \quad (2)$$

where θ is the rotor position, $E(\theta,i)$ is the back electromotive force (EMF), and $L(\theta,i)$ is the instantaneous inductance. The mechanical equation of the SRM is deduced as Equation (3) [10].

$$J \times d\omega/dt = T_e - T_L - T_0, \quad \omega = d\theta/dt, \quad (3)$$

where J is the rotational inertia, ω is the rotational angular speed, T_e is the electromagnetic torque, T_L is the load torque, T_0 is the additional torque including friction torque, air resistance torque, etc. In [11] the authors designed and optimized a 12/8 SRM for EVs and hybrid EVs (HEV). Owing to their optimization method, the torque ripple is reduced by 10.2% and the average torque is increased by 2.4% compared to a typical benchmark

design. They have concluded that the most effective way to increase the initial torque is by increasing the rotor diameter.

There are some SRMs available on the market. The U.S. MOTORS[®] brand from Nidec Motor Corporation (St. Louis, MO, USA) supplies series of SRMs from 14.9 kW to 313 kW and 1000 rpm to 4500 rpm [12]. The Kehui International Ltd. company (Mill Studio Crane Mead, UK) produces SRMs from 4 kW to 500 kW and 380 V to 1140 V alternating current (AC) voltage [13]. The company Rocky Mountain Technologies (Basin, MT, USA) produces series of SRMs in three-phase and four-phase [14]. The power range of the four-phase SRMs is from 0.44 kW to 3.43 kW, the power range of the three-phase SRMs is from 12.67 kW to 26.84 kW. The MACCON company (Munich, Germany) provides four-phase SRMs from 0.44 kW to 8.42 kW [15]. The Striatech subsidiary of Teknatool International company (NORTH CLEARWATER, FL, USA) produces SRMs ranging from 750 W to 1.25 kW [16].

2.1. Winding Configurations

The performance of SRMs varies depending on the winding configurations. Figure 2 represents the winding configurations for different reluctance motors [17,18]. A single-layer concentrated (SLC) winding is a configuration where the phase coil is wound on one pole of the stator and each slot has only one coil. It can be configured to the single-layer mutually coupled (SLMC) windings and the SLC windings with a different winding direction. For the SLMC windings in the SRM, the torque is produced by the change of self and mutual inductances. Using the SLC winding in the conventional SRM, the torque is produced by changing of self-inductances [19]. With the double layer mutually coupled (DLMC) winding and the double layer concentrated (DLC) winding, every slot is shared by two coils. When the fully-pitched (FP) configuration is considered, a distributed winding SRM called mutually coupled SRM (MCSRSM) is used. For some pole and stator phase combinations, SLMC and DLC may not be possible. One of the reasons is the unbalanced winding.

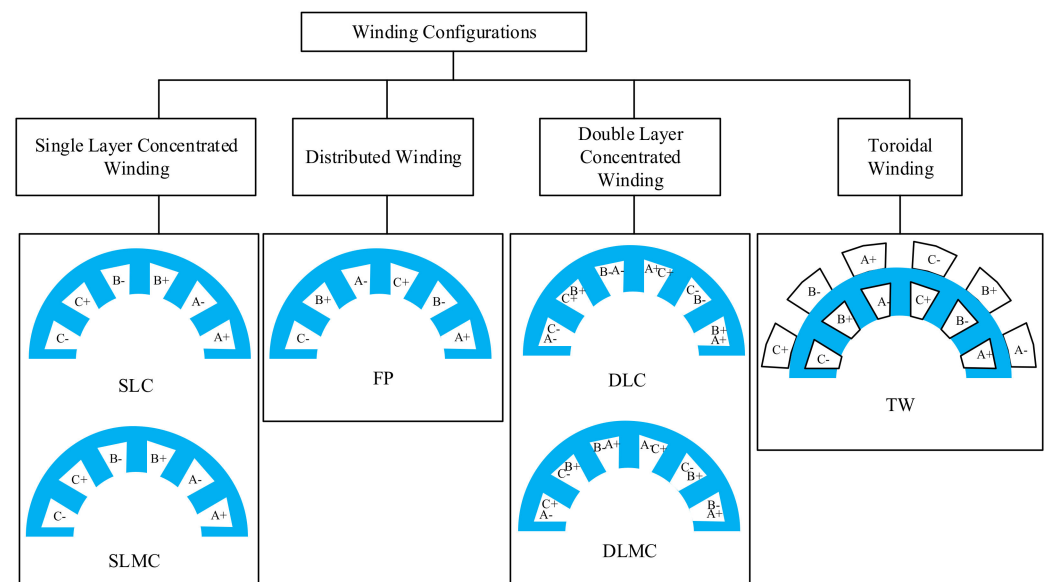


Figure 2. Different winding configurations for switched reluctance motors edited from [17,18].

An unconventional SRM with multiple isolated flux (MIFPs) has been presented to achieve less eddy current and hysteresis losses [20]. The presented SRM has higher torque density than a conventional SRM. A toroidal winding configuration is used for the 12/10 MIFP SRM. The toroidal winding has advantages to improve the heat transfer, to have a wide stator and rotor teeth, to improve the fill factor and to reduce the acoustic noise.

The MCSRSM achieves higher torque performance per ampere at low speeds, and it has a higher back-EMF voltage at high speed [21]. The SRM with the FP winding configurations

can achieve higher average torque and lower torque ripple compared to using the SLC, SLMC, DLC or DLMC windings [17]. A model for toroidal winding SRM (TWSRM) was introduced by [18]. The TWSRM provides additional winding space and keeps the advantages of mutual coupling excitation. It produces more concentrated magnetomotive force (MMF) than the MCSRSM. In addition, it is more sensitive according to saturation. Among the SRMs, the MCSRSM produces the highest torque in the high-speed region, and the TWSRM produces the highest torque in the low-speed region [18].

The comparison results of different winding configurations based on 2D finite element analysis (FEA) are illustrated in Figure 3. The doubly salient reluctance machine (DSRM) in Figure 3 is the SRM supplied with three-phase sinewave currents [17]. The average torque and the torque ripples are compared for different winding configurations at different current levels. Figure 3a presents the average torque comparison of the 12/4 DSRM with different winding configurations. Figure 3b presents the torque ripple comparison of the 12/4 DSRM. Figure 3c presents the average torque comparison of the 12/8 DSRM with different winding configurations. Figure 3d presents the torque ripple comparison of the 12/8 DSRM. It shows that the 12/4 and 12/8 DSRM with the FP winding configurations achieve the highest average torque and low torque ripple. It is an important reference for the CSRSM.

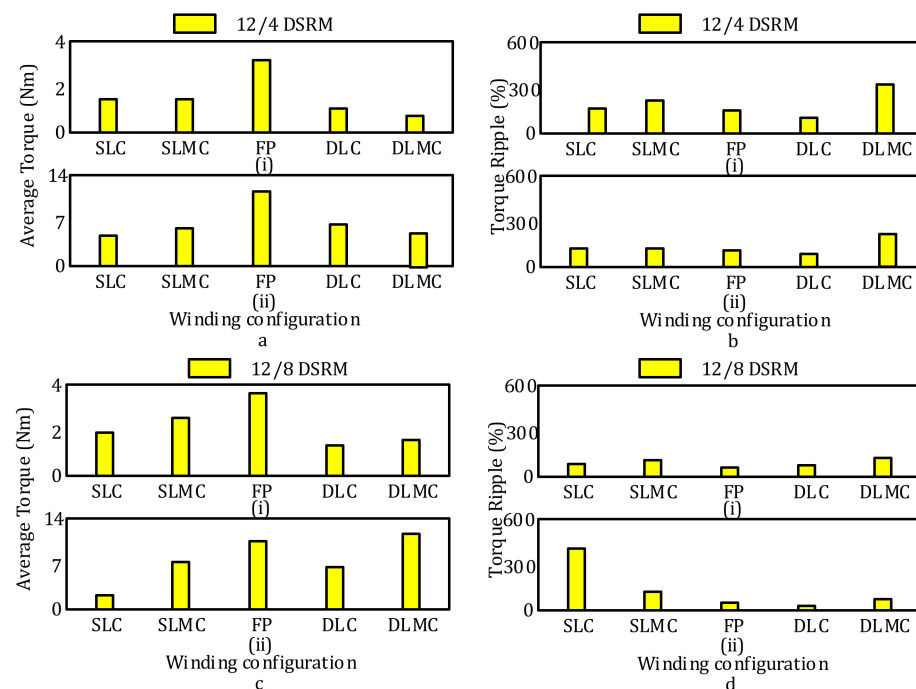


Figure 3. Comparison of torque performance with different winding configurations at (i) 10 Arms and (ii) 40 Arms (a) Average torque of 12/4 machines, (b) Torque ripple coefficient 12/4 machine, (c) Average torque of 12/8 machines, (d) Torque ripple coefficient of 12/8 machines [17].

2.2. One-Stack Structure Conventional SRM

The authors of [22] have analyzed the radial electromagnetic force's spatial distribution and the force's frequencies under eccentricity condition. For the unbalanced magnetic force (UMF), a compensation method has been investigated. The finite element model analysis is used to verify the compensation method. The results have shown that the control method can suppress the UMF in one revolution and decreases the UMF by 80%. Based on the developed flux modulation principle, the publication [23] proposed an advanced current control technique for three-phase SRMs, which can suppress the current harmonics. The torque ripple and motor vibration can be significantly reduced compared to the existing SRM control technique. It improves the robustness of the motor system even without changing the winding arrangement and motor structure [23].

A new online optimization and commutation strategy was presented in [24]. The torque ripple coefficient and efficiency are used to create an objective function. In order to maximize the value of the objective function, the defined boundary angles are optimized online by the genetic algorithm during the operation of the machine. Simulation and experimental results confirm the effectiveness of the method under different operating conditions. An improved torque hysteresis control method is adopted to enhance the efficiency of the SRM. In order to investigate the rotor dynamic characteristics and the mechanical strength of the SRM rotor in high-speed and high-power condition, an investigation scheme has been presented in [25]. The strength of the rotor is verified at 1.2 times the rated speed and the von-Mises yield criterion is used. The conventional method is used to compare with the proposed scheme. It has been proved that the proposed critical speed calculation scheme is more effective and accurate. To achieve the best performance of the SRM, [26] has presented an advanced multi-objective optimization method for the system level. The average output torque, average loss, and torque ripple are the three optimization objectives. The optimized SRM drive system has higher efficiency and lower torque ripple compared to the conventional method. It has been shown that the proposed optimization method is more efficient [26].

In [7], the influence of different pole head shapes on the motor performance in an SRM has been analyzed. The radial force causes vibration in the stator and acoustic noise. The radial force has been reduced by about 19% at the rated current as compared to a standard SRM thanks to a novel pole head shape. It is figured out that the torque ripple has increased by 3.29%. A concept to extend the base speed of the SRM from the perspective of the motor's design has been introduced in [27]. The back EMF can be effectively diminished with the reduction of the motor's saliency. Based on the proposed method, the SRM can achieve wider constant torque range and extended speed range.

The possible demagnetization effect of the low-cost permanent magnet and the influence of Alnico magnets on motor performance have been analyzed in [28]. The result showed that a 3% efficiency improvement has been obtained at the rated operation conditions compared to a same-size SRM. The overall results illustrated that the PM-SRM drive has increased performance, and it has advantages to be used in future motor drive technology.

2.3. Multi-Stack and Multi-Layer Structure Conventional SRM

The multi-stack structure is an approach to cut down on the torque ripple of the SRMs. Different multi-stack solutions are introduced for the CSRSM and the segSRM. Many CSRSMs with multi-stack structure have been investigated in recent years. In [29], a three-stack SRM was presented. Figure 4a shows the structure of the three-stack SRMs. The rotor of each stack is rotated at 15 mechanical degrees from the adjacent one. Compared to the CSRSM, the presented SRM has significant torque quality improvement. In [30], a two-stack SRM has been proposed. Figure 4b illustrates the proposed two-stack SRM. The torque ripple and the vibrations are reduced, and the starting torque is increased compared to a CSRSM. In [31], a two-stack SRM is introduced with a double-layer per phase. In [29], a 6/4 two-stack SRM has been introduced. In [32], a 4-layer SRM was introduced. In [33], two field-assisted switched reluctance generators (SRGs) have been compared. They both have a two-stack structure and the 3D structure. In [34], a two-layer field SRG has been introduced.

In [5], a double-layer per-phase isolated SRM was proposed. Compared to the CSRSM, the proposed SRM is easier to produce due to the geometry factor: it is easier to configure to any number of phases. In [35], a two-stack SRM was introduced, which can achieve a torque ripple reduction. The two-stack SRM from publication [36] achieved a torque ripple reduction. Four-layer SRMs have been introduced in [37–39]; they have a reduced torque ripple. A two-layer switched reluctance motor/generator has been introduced by [40]. The publication [41] proposed a three-stack SRM. Compared to the CSRSM, the proposed SRM has 10% higher efficiency. A seven-stack SRM has been proposed in [42]. Compared to the CSRSM, the proposed SRM has about two times the torque value, less torque ripple and higher efficiency. The publication [43] introduced a seven-layers SRM. Compared to

the CSRSM, the proposed SRM has higher torque at lower speeds, less vibration and noise and 9.5% higher efficiency at the rated speed. The two-stack two-phase SRM with start-up capability has been presented in [44].

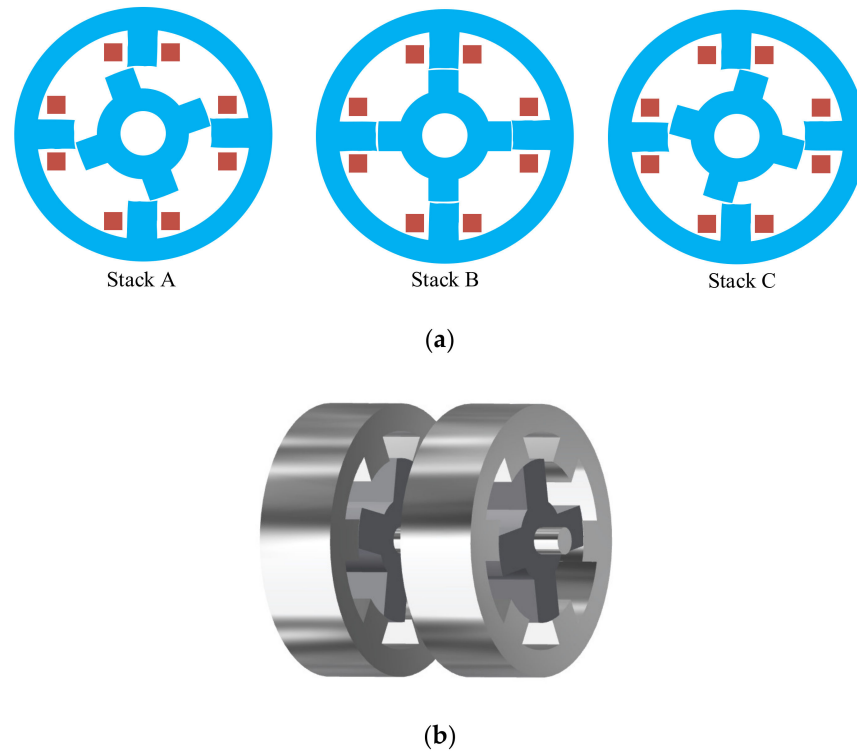


Figure 4. Multi-stack conventional SRMs: (a) A three-stack conventional SRM; (b) A two-stack conventional SRM.

In [45] a multi-stack SRM is proposed with an axially shifted rotor. A new four phase 8/6 SRM with two layer structure is proposed in [46] with a combined generator. In [6] a 16/6 SRM is introduced with segmented hybrid rotor teeth. In addition, it introduced the SRM in the 2D structure that the segmental teeth have been separated into suspension teeth and torque teeth. The suspension teeth produce suspension force, which is used to reduce the force on the position of the bearing. The suspension force and torque force are decoupled. In [47], a developed circuit has been illustrated with accurate results compared to those issued from FEM. It has shown that compared to the FEM, a large calculation time is saved with this method and for preliminary design stages. The time saving property is a valuable factor. A multi-layer SRM has been proposed in [48]. The simulation results from the FEM have shown that the existence of an angular rotation between two adjacent rotors could decrease the torque ripple of the multi-layer SRM significantly while keeping the average torque constant.

2.4. Summary and Comparison of Conventional SRMs

The three-stack SRM introduced in [49] has significant torque quality improvement compared to a CSRSM. Compared to a CSRSM, the two-stack standard SRM proposed in [30] has shown a torque ripple decrease, vibration decrease and starting torque increase. The proposed double-layer-per-phase isolated SRM (DLPISRSM) in [5] has been concluded to be easier to produce and easier to configure to any number of phases. The three-stack SRM developed in [41] presented 10% higher efficiency than a CSRSM. A seven-stack SRM in [42] has shown higher torque, less torque ripple and higher efficiency. Another seven-layer SRM has been proposed in [43] and it has shown higher torque than a CSRSM. The two-stack SRM in [44] has bidirectional startup capability. Compared to a Toyota Prius motor, the proposed SRM in [8] has presented 3 Nm higher torque with similar performance for

the rest. The multi-layer SRM proposed in [46] reduced the torque ripple significantly compared to a CSRSM. The two-stack SRM introduced in [50] had higher torque and lower torque ripple than a CSRSM. In general, the multi-structure SRM has lower torque ripples than the conventional SRM. The one-stack and multi-stack SRM structures are summarized in Table 1.

Table 1. Conventional SRM comparison according to stack structure.

Proposed SRM	Compared SRM	Comparison Parameters	Conclusion	Reference
A three-stack SRM	CSRSM	Torque quality	The proposed motor has significant torque quality improvement.	[49]
Two-stack standard SRM	CSRSM	Torque ripple, vibration and starting torque	The proposed two-stack SRM has a torque ripple decrease, vibration decrease and starting torque increase.	[30]
Double-layer-per-phase isolated SRM (DLPISRSM)	CSRSM	Geometry	The proposed SRM is easier to produce and easier to configure to any number of phases.	[5]
Three-stack SRM	CSRSM	Efficiency	The proposed SRM has more than 10 percent higher efficiency.	[41]
Seven-stack SRM	CSRSM	Torque, efficiency and torque ripple	The proposed SRM has double torque, less torque ripple and higher efficiency	[42]
Seven-layer SRM	CSRSM	Average torque, torque ripple and efficiency	The proposed SRM has higher torque at low speed, less vibration and noise, higher efficiency.	[43]
Two-stack SRM	CSRSM	Start-up capability	The proposed SRM has bidirectional startup capability.	[44]
Seven-stack SRM	A Toyota Prius motor	Torque, efficiency and cooling operation	The proposed SRM has 3 Nm with more torque and easier cooling operation. The efficiency is almost identical.	[8]
Multi-layer SRM	CSRSM	Torque ripple	The torque ripple of the proposed SRM is reduced significantly.	[46]
Two-stack SRM	CSRSM	Average torque and torque ripple	The proposed SRM has higher torque and lower torque ripple.	[50]

3. Segmental Switched Reluctance Motor

The segSRM has been developed in [51,52]. It was shown that much greater force density is possible with the segmental rotor structure [51]. The multi-stack structure is a typical approach to minimize torque ripple. The segmental rotor consists of silicon steel sheet segments and usually an aluminum support block. These segments are attached to this aluminum block. Figure 5 presents the conventional rotor and some examples of segmental rotors. A double-stator switched reluctance machine (DSSRM) has been proposed in [53]. This DSSRM uses a segmental rotor. Figure 5 shows a type of rotor for DSSRM. As shown in the figure, relatively large gaps between rotor segments are observed in that DSSRM rotor compared to other types of segmental SRMs. Nonferromagnetic material is used to fill in the gaps and connect the segments. The segments are connected from both sides of the rotor. Two stators are designed and employed. The two stators are inside and outside of the rotor. A comprehensive comparison showed that the proposed DSSRM has superior performance compared to the CSRSM [53]. Compared to segmental SRM, DSSRM increases the torque density, energy conversion ratio and power factor [54].

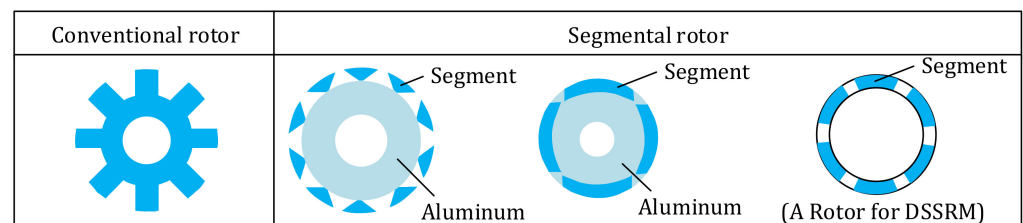


Figure 5. Different rotor structure of an SRM.

As the segments are assembled onto a non-magnetic shaft, the segmental rotor has both more complex structure to fabricate and the weakness of mechanical strength [55]. Aluminum block is usually used as the non-magnetic shaft. The eddy current loss in the aluminum block affects the efficiency of the SRM [55].

3.1. One-Stack Structure of the segSRM

A comparison between the segmental SRM (segSRM) and the CSRSM was performed in [56]. Their result showed that the segSRM produces about 10% higher rated torque throughout the entire speed range and creates less core loss and less copper loss compared to the CSRSM.

In [57], an advanced four-phase belt-driven starter generator 16/10 segmented SRM has been proposed to increase the fault tolerance capability and reduce the torque ripple. A digital control system has been designed and presented for the machine. A DSSRM with the segmental rotor and E-core stators has been proposed in [58] for high-torque applications. The proposed DSSRM has shown higher torque than the single-stator SRM at the same current. Figure 6 gives the one-stack segSRM cross-section illustration [52].

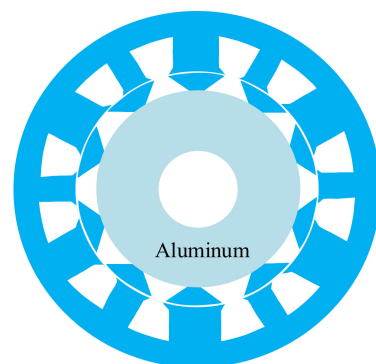


Figure 6. One-stack segmental SRM.

3.2. Multi-Stack and Multi-Layer Structure Segmental SRM

In [59,60], the multi-stack SRMs are presented with the shifted segmental rotor. A performance comparison has been conducted with regard to the CSRSM. The result has shown that the average torque decreased by 10% and the torque ripple decreased by 19%. Figure 7 shows the structure of the segSRM. The authors in [61] introduced an FP 12/4 six-phase SRM with the segmental rotor, as shown in Figure 8. 15-degree shift is designed for the rotor segments. Using the segmental rotor and shifted design, it produced 29.3% higher average torque and reduced the torque ripple by 6.5% compared to a conventional 12/10 SRM. The structures of segmental SRMs that were introduced above are listed in Table 2.



Figure 7. Structure of the multi-stack segSRM edited from [60].

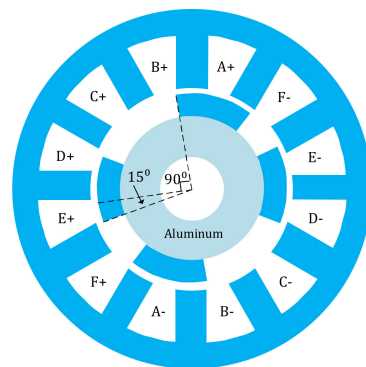


Figure 8. Multi-stack segSRM edited from [61].

Table 2. One-stack and multi-stack segmental SRMs.

Proposed SRM	Compared SRM	Comparison Parameters	Conclusion	Reference
SRM with segmental rotor	CSRM	Average torque	The proposed SRM with segmental rotor has significant higher torque per copper loss than CSRM	[51]
SRM with segmental rotor	CSRM	Average torque	The proposed SRM with segmental rotor has 44% higher torque than a CSRM.	[52]
SRM with segmental rotor	CSRM	Average torque	The proposed SRMs with segmental rotor have over 40% higher torque than a CSRM.	[62]
SRM with segmental rotor	CSRM	Average torque	Compared to the CSRM, the proposed SRM with segmental rotor produces much higher average torque.	[56]
A two-stack SRM with segmental rotor	CSRM	Average torque, torque ripple	The proposed SRM obtains 19% torque ripple decrease and 10% average torque decrease.	[59]
A two-stack SRM with segmental rotor	CSRM	Torque ripple and vibration	The proposed SRM obtains 10% average torque decrease and 19% torque ripple decrease.	[60]
SRM with shifted segmental rotor	CSRM	Average torque, torque ripple	The proposed SRM has 6.5% lower torque ripple and 29.3% higher average torque than the CSRM.	[61]

It is necessary to mention that with a short flux path configuration, it is possible to design an equivalent multi-stack structure in the 2D [61]. The 2D structure is simpler for fabrication and analysis. Figure 9 shows the excitation method of the proposed SRM.

It has two phases working at any time which produces higher average torque than the conventional six-phase SRM.

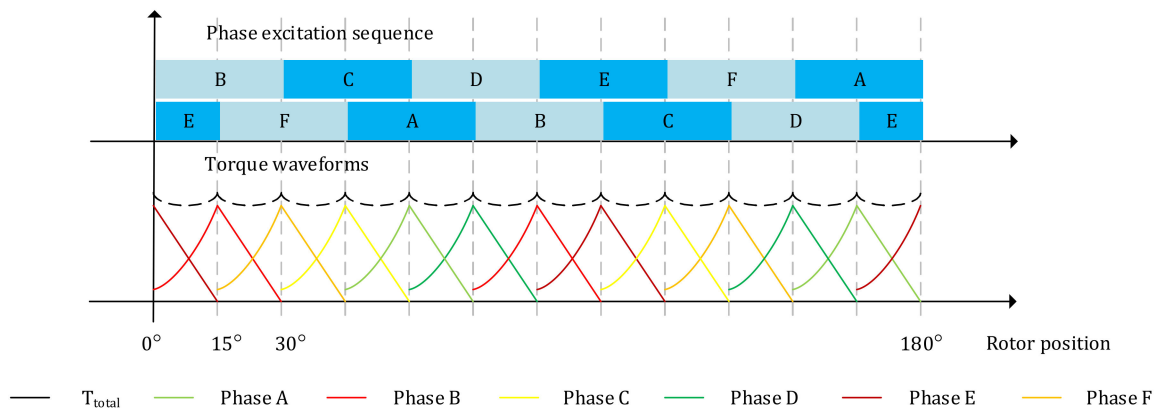


Figure 9. Working process of the proposed SRM in [61].

Figure 10 shows the dynamic simulation results of the proposed SRM and reference SRMs at 2750 rpm rated speed and at rated current. The SRM1 is the reference 12/10 conventional SRM, the SRM2 is the reference 12/10 segSRM, and the SRM3 is the proposed 12/4 segSRM.

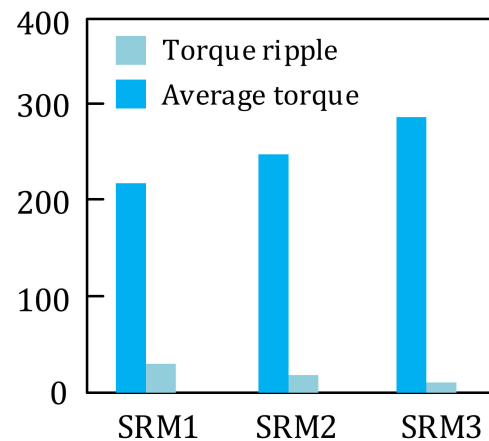


Figure 10. Dynamic simulation results of the proposed SRM in [61].

The simulation results have shown that the proposed SRM has higher average torque and lower torque ripple. The proposed SRM had 29.3% higher average torque than the referenced conventional 12/10 SRM and 16.2% higher average torque than the referenced segmental 12/10 SRM. Also, it had 6.5% lower torque ripple than the referenced conventional 12/10 SRM and 2.0% lower torque ripple than the referenced 12/10 segmental SRM.

3.3. Summary and Comparison of Segmental Structures

Table 2 presents the summary of different one-stack and multi-stack SRMs with the segmental rotor. In [51], an SRM with the segmental rotor was proposed. Compared to the CSRSM, the proposed SRM with a segmental rotor had significantly higher torque than the CSRSM. The proposed SRM with segmental rotor had over 40% higher torque than the CSRSM regarding the same winding loss in the theoretical analyses study in [62]. In [56], the SRM with the segmental rotor produced much higher average torque compared to the CSRSM. The two-stack SRM with segmental rotor introduced in [59] obtained 19% torque ripple reduction and 10% average torque increase. The new two-stack SRM with the segmental rotor developed in [60] achieved 10% average torque decrease and 19% torque

ripple decrease compared to CSRSM. The SRM with shifted segmental rotor proposed in [61] had 6.5% lower torque ripple and 29.3% higher average torque.

4. Drive of the SRM

Power electronic drives are the basic electronic systems used for operating electrical machines such as SRMs. The drives of the SRMs used along with suitable control method supply the desired electrical outputs for the machine windings [63]. Hence, the drive is highly influential to the performance of an SRM.

4.1. Conventional Converters for SRMs

Figures 11 and 12 classify the switched reluctance (SR) converter by phase switch and commutation type [64,65], with q representing the number of phases for the motor. Differences between converters have been investigated in [66]. Five categories are classified by phase switch: single switch converter, $(q + 1)$ switch converter, 1.5 switch/phase converter, two switch/phase converter, $(2q + 1)$ switch converter and another category is the two-stage power converter. With this classification, it is convenient to calculate the number of switches and design the converter based on the number of switches. There are four types of commutation methods presented in Figure 12: dissipative, magnetic, resonant and capacitive.

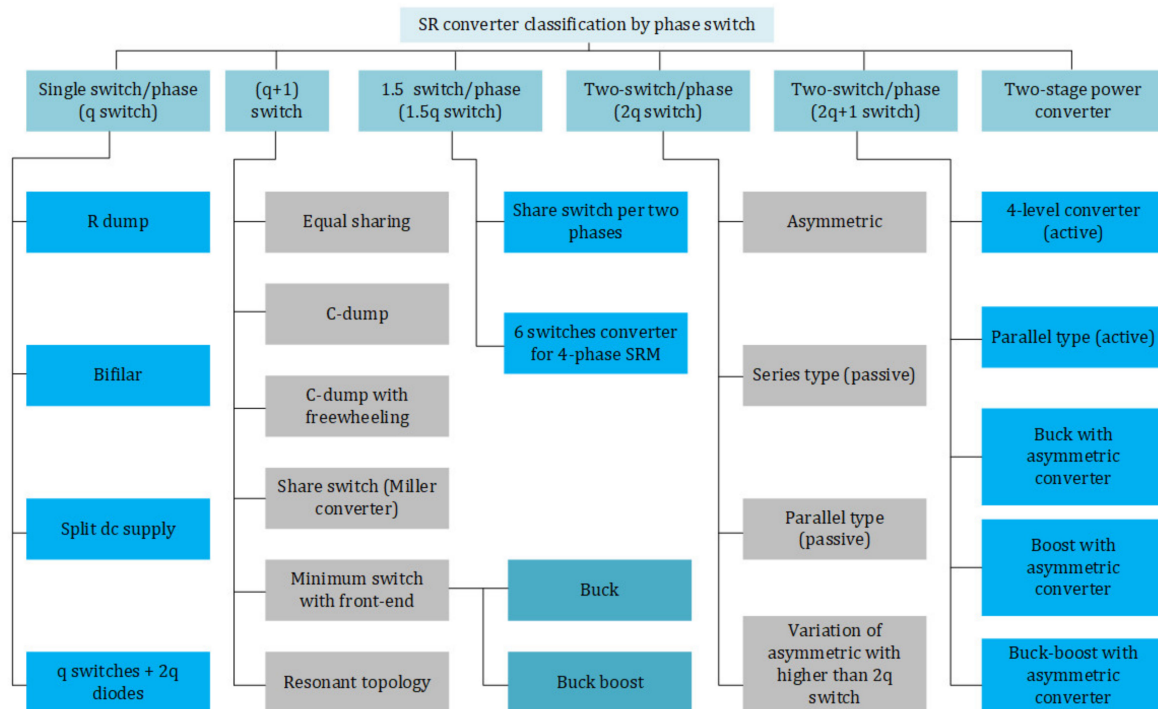


Figure 11. SR converter configuration by phase switch edited from [64].

Illustrations of the most common types of SR converter are presented in Figure 13. The phase A in Figure 13 is the phase winding of the SRM. The dissipative type converter dissipates the stored magnetic energy with a resistor. Figure 13a presents the circuit of an R-dump dissipative converter. The advantages of this converter are the simple circuit, the small number of semiconductor components and low cost. The stored magnetic energy is transferred to a closely coupled second winding with the magnetic converters. Figure 13b displays the bifilar magnetic converter. The major advantage of this converter is a simple topology. The disadvantage is that the motor power density of this converter is lower than the motor with the conventional converter. The resonant type converter has an inductance for a buck, boost or resonant function. Figure 13c illustrates the C-dump resonant SR

converter. The advantage of the resonant SR converter is that the phase winding voltage can work with a snubber circuit. One disadvantage is that adding the inductor will increase the size, weight and cost of the converter. Finally, the capacitive converter stores the magnetic energy in capacitors. Figure 13d shows the asymmetric bridge capacitive SR converter. The stored energy can be fed back with the inductance of the phase winding. It makes the capacitive converter more effective [64]. The disadvantage is that the capacitor increases the loss of the converter.

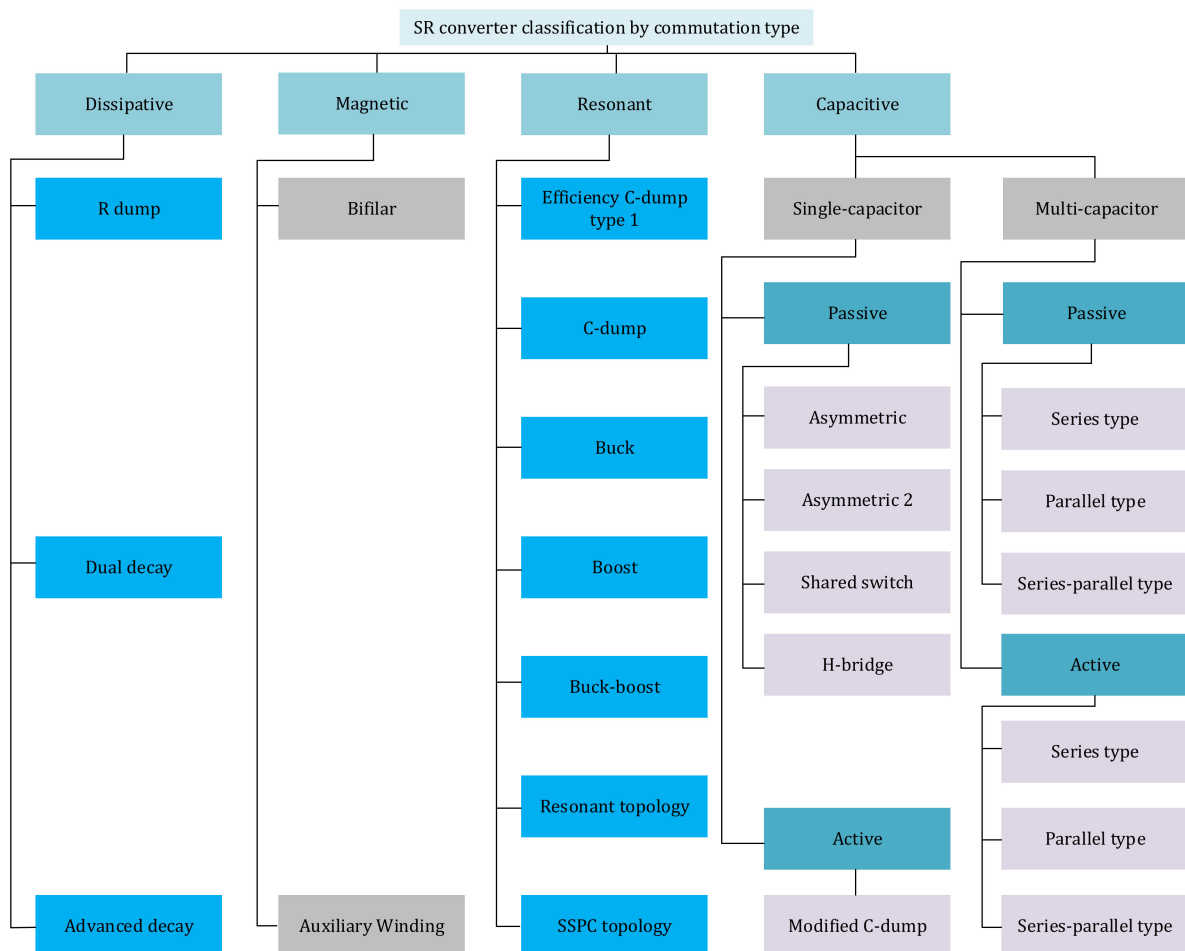


Figure 12. SR converter configuration by commutation type edited from [64].

In [67], conventional power system risk and reliability indicators of loss of load expectation (LOLE) have been used to qualify the reliability of a power electronic based power system (PEPS). The reliability functions are based on the physics of failure (PoF). In order to evaluate the level of the reliability of the PEPS with non-constant failure rates, the Markov chain approach is employed, based on a piece-wise solution. The SiC MOSFET switching characteristic with the highly inductive environment has been investigated in [68]. The characteristic product of stray-inductance with nominal current grows with the power rating, and it is a limiting factor for the speed of current commutation. The impact of the reduction on switching on/off time is analyzed together with its influence on switching speed. In [69], a new control for the SRG drive by a wind power generation system has been proposed. With this novel drive, the output power of the generator is maximized from three aspects. Maximum use of the negative slope area of the phase inductance in generating mode, keeping the current in flat-top mode at any speed and reducing the rise-up time of the phase current. In [69], a buck converter fed SRM drive was proposed. It has the capability to suppress torque ripples and improve the power factor. An

appropriate DC-link voltage is applied to reduce the torque ripple with the buck converter. Furthermore, a function of power factor correction is realized at the AC side. This buck converter is used to improve power quality. Consequently, an enhanced performance has been reached for the speed control. The results in [70] illustrated that the proposed drive performs power factor correction and suppresses the torque ripple. An enhanced control approach and an integrated converter model for torque ripple minimization of the SRM have been proposed in [71]. The proposed method has a better performing controller which supply less torque ripple and shorter settling time as compared to other techniques.

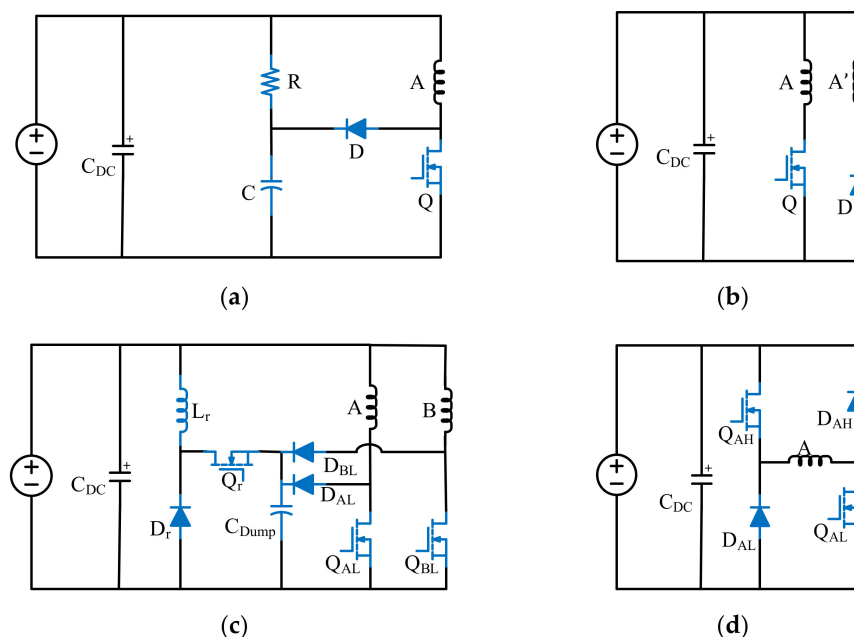


Figure 13. SR converters: (a) R-dump dissipative converter; (b) Bifilar magnetic converter; (c) C-dump resonant converter; (d) Asymmetric single capacitor type capacitive converter.

4.2. Soft-Switching Converters for the SRM

The soft-switching technique reduces the switching losses for the SRM drive. Different soft-switched converters have been developed for the SRMs, and they were assessed in [72]. Figure 14 lists the soft-switched converters for SRMs, with a single subgroup of self-commutating converters: series resonant converters, zero-voltage transition (ZVT) PWM converters, auxiliary quasi-resonant DC-link (AQRDCL) converters, current source converters and H-bridge converters.

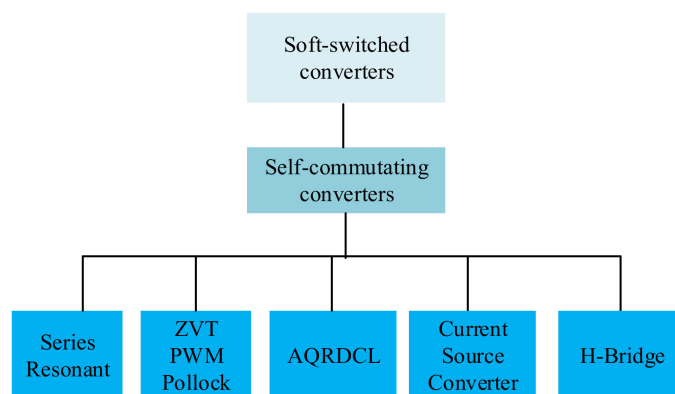


Figure 14. Soft-switched converters edited from [72].

The series resonant converter has two modes of operation: magnetization and demagnetization. The main advantage of this converter is reducing the switching losses and voltage stress in the switching components. The main disadvantages are that the number of components is high, and it increases the system cost. The ZVT PWM converter regulates the DC-link voltage using a chopping switch and an auxiliary switch. The chopping switch creates conduction losses. Independent current control of the phase windings has some limitations with this converter. The AQRDCL converter makes the main switches transition occurring at zero volts with a resonant circuit.

The main disadvantage is that the resonant circuit switches cause conduction losses and the zero voltage switching limits the independent phase control. In the H-bridge soft-switched converter, two phases must always carry current. The main advantage is that it reduces the cost of the converter components by allowing one switch and one diode per phase. The main disadvantages include that it prevents independent phase control, and the number of phases must be a multiple of four phases. Figure 15 displays the H-bridge soft-switched converter.

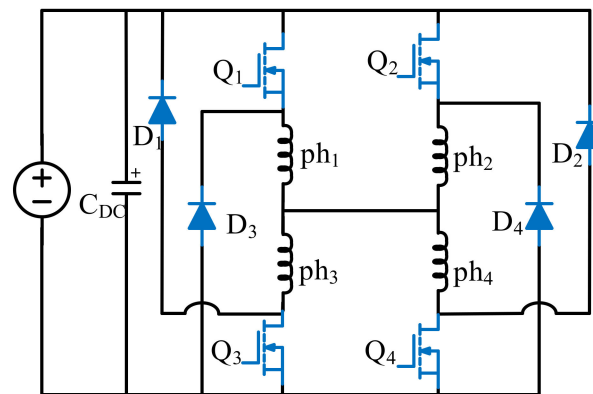


Figure 15. H-bridge soft-switched converter.

4.3. SRM Drive with Three-Phase Standard Six-Switch Inverter

With standard inverters, the main advantages are a reduction of the drive size and increasing usage in commercial applications. In [73], a three-phase standard six-switch inverter has been used to construct the drive for a three-phase SRM. New hybrid winding topologies are proposed. Compared to an SRM with the conventional drive, the proposed SRM has higher power density, higher average torque, higher torque/weight ratio, and lower torque ripple. In [74], an SRM with the conventional stator and segmental rotor has been proposed, which is driven by a three-phase standard inverter. Compared to the conventional SRM, the proposed SRM system results in higher average torque and lower torque ripple. With a three-phase standard inverter, an MCSRM has been designed in [75] for speed extension in the HEV applications. Compared to the CSRM drive, the proposed drive with the standard inverter has a faster adoption in the HEVs. In [76], a new SRM with two three-phase standard inverters has been introduced and analyzed. The proposed drive can overcome the fault of top or bottom power switches in a leg without changing current amplitudes in healthy phases.

4.4. Integrated EV Battery Chargers for the SRM

By reutilization of existing power electronics components in the SRM drives, researchers proposed the idea of an integrated EV battery charger already more than thirty years ago [77]. With the integrated charger, the vehicles have less weight compared to a separate on-board charger. The topologies of on-board integrated chargers have been reviewed, and a new single-phase integrated charger with the quasi-Z-source network has been introduced in [78]. The introduced integrated charger has advantages such as smaller inductors and capacitors and the fact of using the motor winding as a filter inductor for

grid-side distortions. However, there are some disadvantages for the integrated charger, for instance, mechanical structures or control methods are needed to block the motor from rotation and the traction system may limit the charging power.

In [79], two three-phase standard intelligent power modules (IPM) were utilized to construct the SRM drive and integrated charger. When charging, the IPM embedded power devices and the SRM windings are used to form the buck-boost or the buck PFC charger. The advantage is that standard power modules are used. It reduces the cost to develop the charger and motor drive. The disadvantages are that modifications are needed to drive the SRM in the high-speed application for the EVs. Reference [80] has developed an integrated SRM drive with battery charging capability for the EV applications. A Miller converter is used, in which one PWM switch is used to replace four switches, which makes the developed integrated drive compact. On the other hand, the torque ripple is an issue and should be reduced by control methods in driving mode. A novel integrated charger with a central-tapped winding for the SRM drive was proposed by [81]. A three-phase full-bridge drive and motor winding in the central-tapped configuration are used to build the SRM drive with charging capability. The disadvantage is that an additional relay is needed compared to the conventional drive system.

In [82], a new integrated SRM drive with split-winding for battery charger was designed and simulated. It has a simple structure, but the force of the rotor is unbalanced. There is a need to lock the rotor in charging mode. A supercapacitor discharger converter and a bidirectional battery charger/discharger converter were used to build the integrated battery charger in [83]. In driving mode, the driver provides two voltage levels for magnetization and demagnetization. In [84], a new integrated SRM drive with a battery charger was designed, simulated and analyzed. The integrated SRM drive is made up of a simple structure. However, a zero-torque control is needed for the SRM drive. A bridgeless interleaved (BLIL) boost converter was designed in [85]. By adding a small number of components, an integrated driver is designed. It can be used as a BLIL boost converter, buck-boost converter, and interleaved boost converter to realize the charging function. The PFC charging function is integrated to avoid a front-end AC-DC PFC converter. The interleaving operation is allowed during charging mode to cancel the ripples of input inductance currents from two parallel boost converters. Besides, the photovoltaic (PV) charging function is realized. In [86], the constant current constant voltage (CCCV) control method was used with a hybrid power source integrated battery charger with an SRM drive. It has the function to charge the battery from PV with the maximum power point tracking (MPPT) method. In [87], the combination of asymmetric bridge and half bridge (A + HB) were introduced to construct the integrated inverter with no need to modify the motor. Three additional IGBTs, five additional diodes and two relays are needed. A novel integrated power converter (NIPC) with fewer devices and higher reliability was proposed in [88]. It is suitable for any SRM with various phases. The static and dynamic performance are not worse than asymmetric half-bridge power converter (AHBPC). The voltage stress of the reliability-critical MOSFETs is low with the proposed control method. But the torque ripple can be reduced further with optimized working modes.

In [89], an integrated SRM drive with two current sensors was designed for driving/charging/discharging functions. There is no extra component, sensor and mode selection needed for the driver. A modular multilevel converter (MMC) based drive was proposed for the SRM with a decentralized battery energy storage system (BESS) for the HEV applications in [90]. The DC bus voltage can be controlled compared to the conventional SRM drives. Multilevel phase voltage can be obtained in the demagnetization stage to get better torque capability. It can be constructed as a modular structure. Flexible charging and fault-tolerance ability are achieved. With the SRM winding, a three-channel interleaved boost converter was designed in [91]. The power factor correction (PFC) is realized in the integrated drive. It is not needed to add external power electronics components. In [92], an integrated SRM with driving and charging functions for the SRM was proposed for the EV application. The advantage is that there is no need to add external inductors

and charging units. An electrified powertrain with the SRM (both motors and generators) in the HEV application was proposed and analyzed in [93]. Compared to the conventional asymmetrical half-bridge drive, the integrated drive has less power devices. The different integrated EV chargers with SRM drives literature review findings are summarized in Table 3.

Table 3. Summary of the integrated charger with SRM drive.

Adopted Technique	Details	Advantage	Disadvantage	Reference
Standard Intelligent Power Module (IPM)	Two three-phase IPMs	Standard power modules are used.	Suitable modifications are needed to drive the SRM in high-speed application for EVs	[79]
Miller converter	A Miller converter	The SRM drive is compact.	In driving mode, the torque ripple is an issue and should be reduced by control method.	[80]
Central-tapped winding of SRM and H-bridge	A three-phase full-bridge drive and motor winding in central-tapped	A three-phase full-bridge drive and motor winding in central-tapped are used.	There is an additional relay compared to the conventional drive system.	[81]
Split-winding	A new integrated SRM drive with battery charger	It has a simple structure.	The force of the rotor is unbalanced.	[82]
Supercapacitor	A supercapacitor, a supercapacitor discharger converter and a bidirectional battery charger/discharger converter	The drive provides two voltages for magnetization and demagnetization		[83]
Split-winding	A new integrated SRM drive with battery charger	The integrated SRM drive is in a simple structure.	A zero-torque control is needed for the SRM drive.	[84]
Bridgeless interleaved (BLIL) boost converter	By adding a small number of components, an integrated driver is designed.	The PFC charging function is integrated to avoid front-end AC-DC PFC converter.		[85]
Constant current constant voltage (CCCV)	A hybrid power source integrated battery charger with SRM driver	It has the function to charge the battery from PV with maximum power point tracking (MPPT) method.		[86]
Asymmetric plus half bridge (A + HB) converter	The combination of asymmetric bridge and half bridge (A + HB)	No need to modify the motor.		[87]
Novel integrated power converter (NIPC)	The novel integrated power converter (NIPC) with fewer devices but more reliability	It is suitable for any number of phases SRM.	The torque ripple can be reduced more with optimized working modes.	[88]
Integrated drive with two sensors	An integrated SRM drive with two current sensors for driving/charging/discharging	There is no extra component, sensor and mode selection needed for the drive.		[89]
Modular multilevel converter (MMC)-based drive	A modular multilevel converter (MMC)-based driver with decentralized battery energy storage system (BESS)	The DC bus voltage can be controlled compared to conventional SRM drives.		[90]
An integrated drive for SRM	A three-channel interleaved boost converter	It is not needed to add external power electronics components.		[91]
An integrated drive for SRM	An integrated SRM with driving and charging functions	There is no need to add external inductors and charging units.		[92]
An integrated electrified powertrain for SRG and SRM	An electrified powertrain for SRG and SRM in HEV application	Compared to conventional asymmetrical half-bridge driver, the integrated driver has less power devices.		[93]

5. SRM Control Methods

In this section, the control methods of the SRM are assessed. In [65], the different SRM control methods were discussed. Figure 16 shows a typical SRM torque control block diagram. The T^* is the reference torque. It is divided into three reference torques T_a^* , T_b^* and T_c^* for each phase. The reference currents I_a^* , I_b^* and I_c^* are calculated with a look-up table and controlled with a current controller.

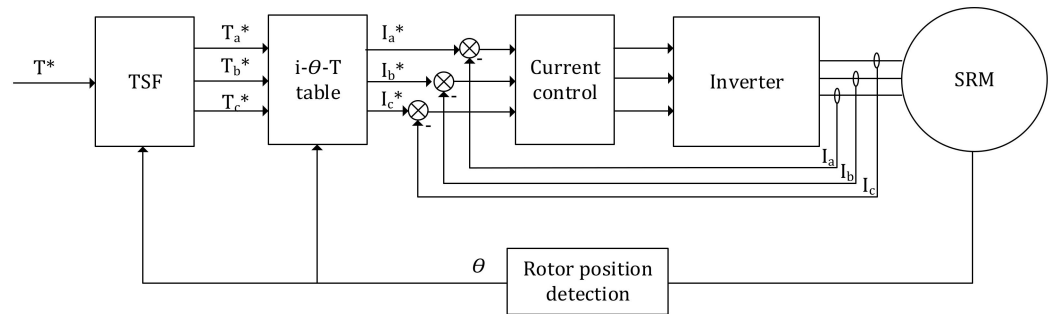


Figure 16. Block diagram of a typical SRM torque control system.

The main control methods of the SRM are angle control, current control, direct instantaneous torque control (DITC), advanced direct instantaneous torque control (ADITC) and torque sharing control with torque sharing function (TSF). Additionally, different control methods are proposed for different purposes, such as low-noise, less torque ripple, higher efficiency or more simple model. Besides, field-oriented control (FOC) for SRM has been researched in [94], where it is concluded that the SRM with FOC driver produces less harmonics than a half-bridge converter and multilevel inverter. These different control methods are reviewed in the following paragraphs. In [4], the control techniques and topologies for the low-noise SRM in the EV applications were reviewed. In [95], the maximum torque-ripple-free speed of the selected offline TSF was confirmed to be seven times higher than the best case in these conventional TSFs. The objective function of an offline TSF is composed of two secondary objectives with a Tikhonov factor to minimize the square of the phase current (copper loss) and derivatives of current references (rate of change of flux linkage). The reference torque for phase k is defined as:

$$T_{\text{ref}(k)} = \begin{cases} 0 & 0 \leq \theta < \theta_{\text{on}} \\ T_{\text{ref}} \times f_{\text{rise}}(\theta) & \theta_{\text{on}} \leq \theta < \theta_{\text{on}} + \theta_{\text{ov}} \\ T_{\text{ref}} & \theta_{\text{on}} + \theta_{\text{ov}} \leq \theta < \theta_{\text{off}} \\ T_{\text{ref}} \times f_{\text{fall}}(\theta) & \theta_{\text{off}} \leq \theta < \theta_{\text{off}} + \theta_{\text{ov}} \\ 0 & \theta_{\text{off}} + \theta_{\text{ov}} \leq \theta < \theta_p \end{cases} \quad (4)$$

where $T_{\text{ref}(k)}$ is the reference torque for phase k , T_{ref} is the total reference torque, $f_{\text{rise}}(\theta)$ is the rising TSF for the previous phase, $f_{\text{fall}}(\theta)$ is the reducing TSF for the next phase, θ_{on} , θ_{off} , θ_{ov} , and θ_p are the turn-on, turn-off, overlapping and rotor pole pitch angle, respectively.

Two performance indicators are defined to evaluate the efficiency and torque-speed performance. They are the rate of change of flux linkage with respect to rotor position and RMS current in each phase for copper loss of the electric machine. The absolute value of the rate of change of flux linkage (ARCFL) should be maximized when considering the copper losses. The ARCFL (M_λ) is defined as:

$$M_\lambda = \max(d\lambda_{\text{rise}}/d\theta, -d\lambda_{\text{fall}}/d\theta), \quad (5)$$

where λ_{rise} is the rising flux linkage from the incoming phase, and λ_{fall} is the reducing flux linkage from the outgoing phase.

The maximum torque-ripple-free speed (TRFS) ω_{\max} can be calculated as in Equation (6), where V_{dc} is the voltage of the dc-link.

$$\omega_{\max} = V_{dc}/M_{\lambda}, \quad (6)$$

The RMS current for copper loss can be calculated as follows:

$$I_{\text{rms}} = \text{sqrt}(1/\theta_p \times (\int (i_k^2)d\theta + \int (i_{k-1}^2)d\theta)), \quad (7)$$

where I_{rms} , i_k , and $i_{(k-1)}$ is the RMS current, phase current at the present state and phase current at the previous state, respectively.

In [95], a reliable and efficient grid supported a solar-powered water pumping system (SPWPS) was proposed. This paper uses a new control logic in the experiment to achieve power quality improvement in terms of total harmonic distortion (THD).

A novel torque ripple minimization method was presented in [96] by using the genetic algorithm (GA). Using the rising and falling angles, instead of overlapping angle, a new sinusoidal TSF is improved to minimize the copper losses and the torque ripple. The method is verified with an experimental test bench. With a hysteresis current controller and digital speed regulator, the chaotic phenomena in the SRM were investigated [97]. The chaotic orbit in the curve of the current and speed is a typical chaotic phenomenon. This paper analyzes different modes of the drive system with simulation methods: fundamental, subharmonic and chaotic operations. The study [98] proposed an active diagnosis of an SRM in a light EV. It uses an average torque estimator and a sliding mode observer (SMO) to build the diagnosis method. If a permanent type of fault is detected, the damaged sensor output will be replaced by the estimated speed and position for continuous operation. Second, all possible stator winding faults will be diagnosed with the co-energy based average torque estimation scheme. With the parameter of the motor measured from the terminals, the average torque of each phase is estimated. As soon as the completion of one electric cycle right after the fault happens, it can be detected effectively.

It has been proven that the torque can be improved by 15% at the rated condition and 20% at light load conditions, compared to the conventional driving method [99]. It is analyzed with analytical and finite element methods. Furthermore, the large torque ripple is suppressed, the core losses are reduced, and the efficiency is improved. The proposed current profile has fixed parameters and can be easily adapted to different machine specifications, compared to many other current profiling methods. In [100], a torque-flux linkage recurrent neural network adaptive inversion control of torque for the SRM was proposed. The proposed method can reduce the torque ripple effectively with recurrent performance.

A second-order sliding mode control of the SRM was proposed in [101]. The proposed method offers a reduction of the torque ripple, the elimination of chattering phenomena and lower harmonic distortion of motor currents. In [102], a continuous control set model predictive control of an SRM using lookup tables was proposed. The proposed method has the fixed switching frequency and less computational load. Based on flux-current locus control, a novel average torque control method of the SRM was proposed by [103]. The proposed controller gets more precise torque and a better energy conversion ratio. Figure 17 shows the controller diagram in [103]. With the reference torque T^* , the next point of flux-linkage, current and position are calculated by an average torque controller. With a micro-step locus controller, the reference flux-linkage Ψ^* and current i^* are calculated. In the next step, the current is controlled with a hybrid flux-current controller.

5.1. Control Method for Torque Ripple Reduction

The current profiling and angle optimization methods are two control methods to reduce torque ripple [4]. In the angle optimization method, the turn-off and turn-on angles are optimized to achieve lower torque ripple. In the current profiling method, modulation of phase current profiles is performed to generate a smoother torque. Furthermore, the

average torque control (ATC) method can be used to estimate the average torque online and suppress the torque ripple to an acceptable level. The direct torque control (DTC) method can be employed to minimize the torque ripple of the SRM. The DITC, which is derived from the DTC, has a rapid response to torque errors. The DITC can reduce the torque ripple more effectively. With a PWM module, the switching frequency of the DTC can be fixed, leading to the PWM-DITC control method. The most common torque control schemes of the SRM are presented in Figure 18.

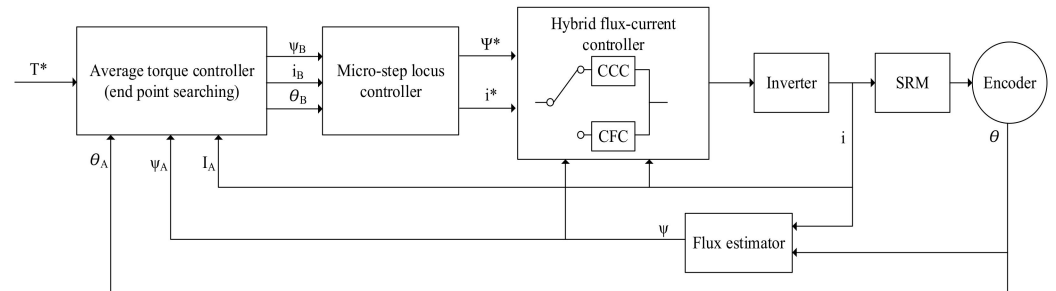
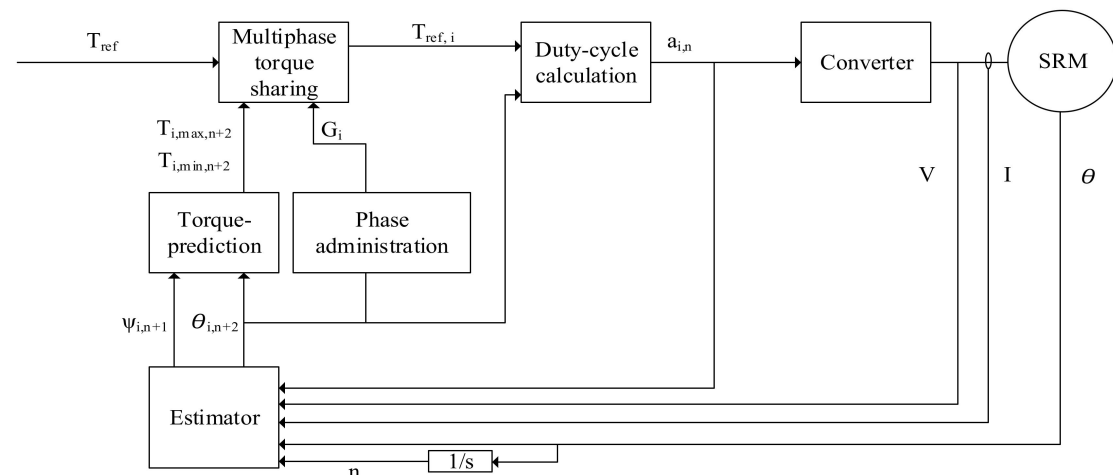
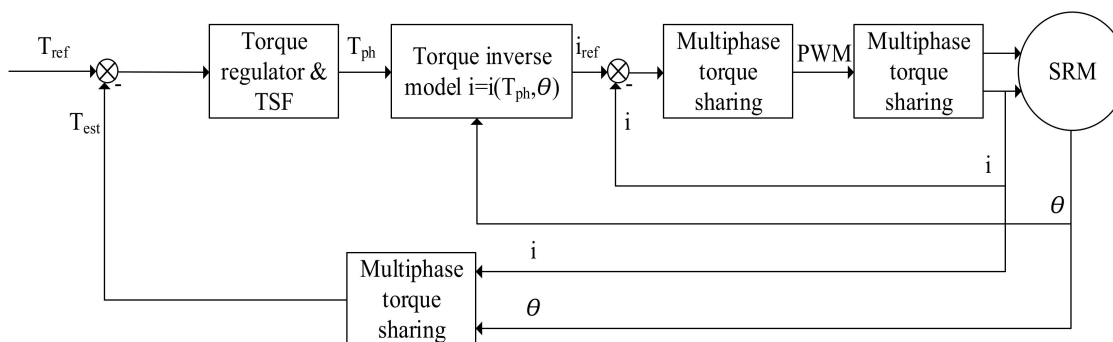


Figure 17. The hybrid flux-current controller diagram for SRM edited from [103].



(a)



(b)

Figure 18. Cont.

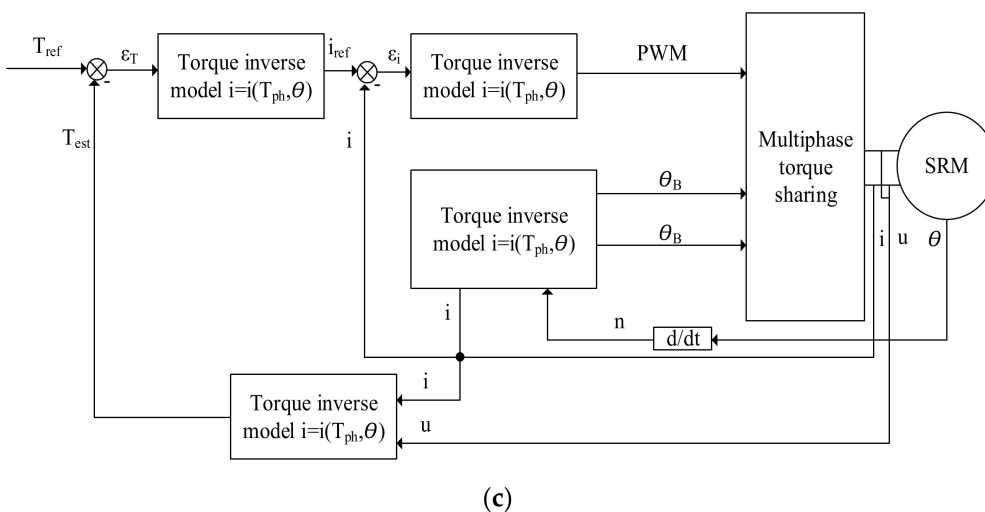


Figure 18. Block diagrams of torque control schemes: (a) PWM-DITC edited from [104]; (b) DITC [105]; (c) ATC [106].

5.2. Fault-Diagnosis and Fault-Tolerance Techniques

The electric motors used in EVs must be resistant to harsh environments and high temperatures. This may result in different fault risks in the motor drive [106,107]. The faults may lead to more failures and cause further damage to other components which were initially not affected because the fault ride-through capability is so critical in the SRM control system [10]. The existing fault diagnosis and fault tolerance approaches are illustrated in Figure 19. There are eight methods for fault diagnosis: hardware assistant, fault flag variable, fault indicator, trial and error, spectrum analysis, coordinate conversion, Kalman filter and digitizing methods. There are also eight methods to increase fault tolerance: multiple inverter configuration, additional phase leg, relay networks, field control, position signal assistance, artificial neural networks, current profiling and the PM assistant methods.

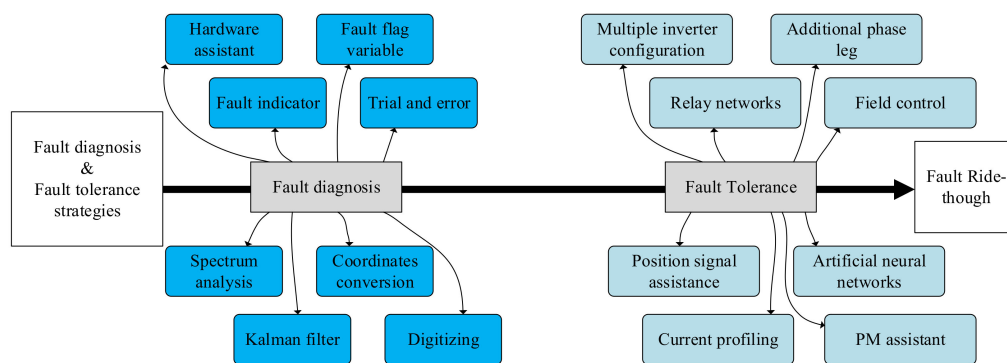


Figure 19. Classification of fault diagnosis and fault tolerant methods edited from [10].

The possible fault types and locations are displayed in Figure 20 [10]. There are five types of faults: converter fault, winding fault, current fault, position sensor fault and eccentricity fault. The first step to achieve the fault ride-through capability is to locate and diagnose the fault in real-time. The second step is to use hardware or software based fault-tolerant control in the motor drives. Redundant components such as relays and switches are often used to bypass faulty parts during the operation. Furthermore, current profiling and artificial neural networks are useful techniques to provide the fault ride-through capability to the motor drives [10].

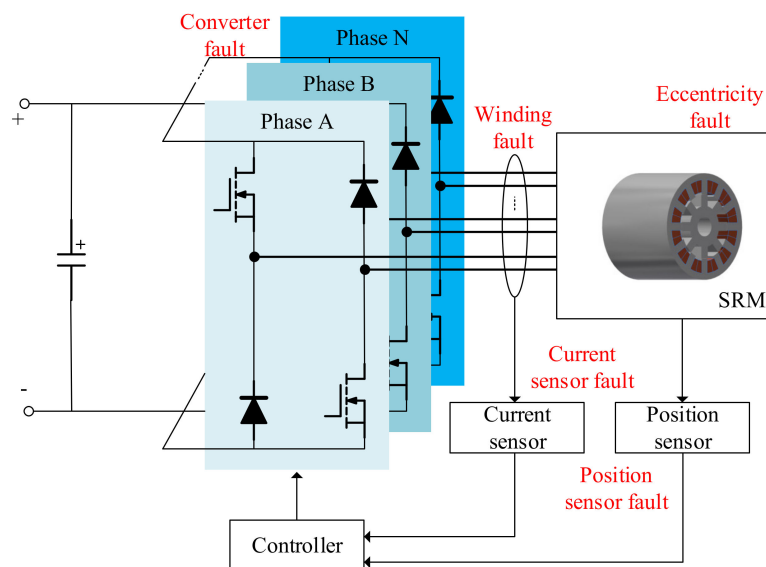


Figure 20. SRM drive system and location of different faults edited from [10].

5.3. Sensorless Control of the SRMs

The sensorless control system of the SRM can reduce the cost of the motor drive system and improve reliability. In [98], a sliding mode observer (SMO) for the fault-tolerance mode was introduced. The SMO based sensorless technique is proposed to estimate the motor speed and the rotor position. The complete progress of sensor fault and winding fault diagnosis are presented in Figure 21. In this progress, the SMO method for the sensor can be used to estimate position and speed for sensorless control [98].

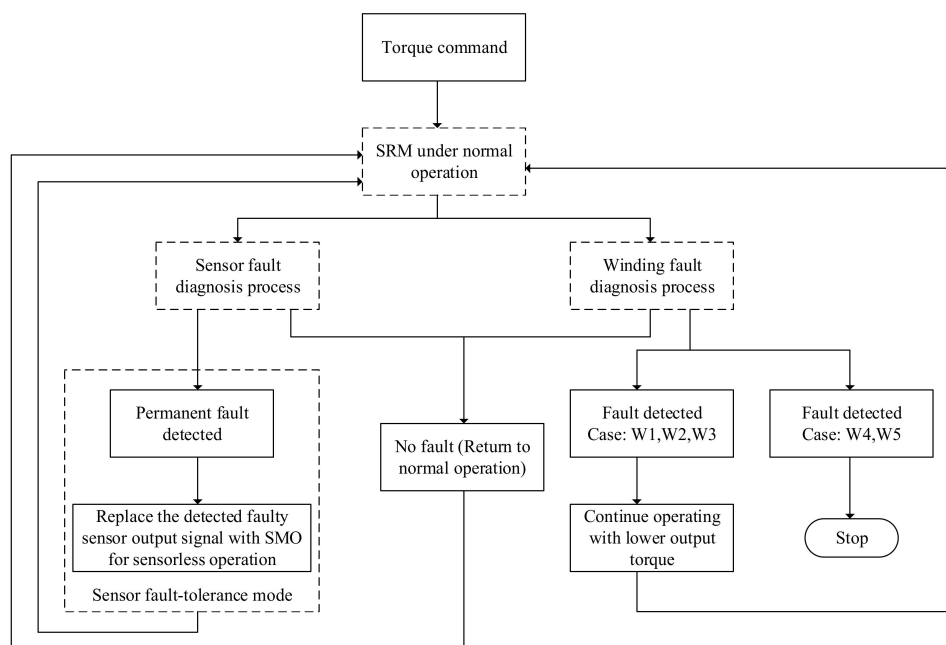


Figure 21. The complete progress of sensor fault and winding fault diagnosis edited from [98].

The torque control strategy for the SRM can be classified into indirect or direct torque control [108]. A complex algorithm or distribution function is used in the indirect torque control to produce the reference current. The torque hysteresis controller and simple control scheme are used in the direct torque control to decrease the torque ripple. The indirect torque control category includes open-loop current profiling method, the TSF method

and the ATC method. The direct torque control method includes the DITC, the ADITC and the PWM-DITC methods. Figure 22 shows the classifications of the torque control strategies [94,108].

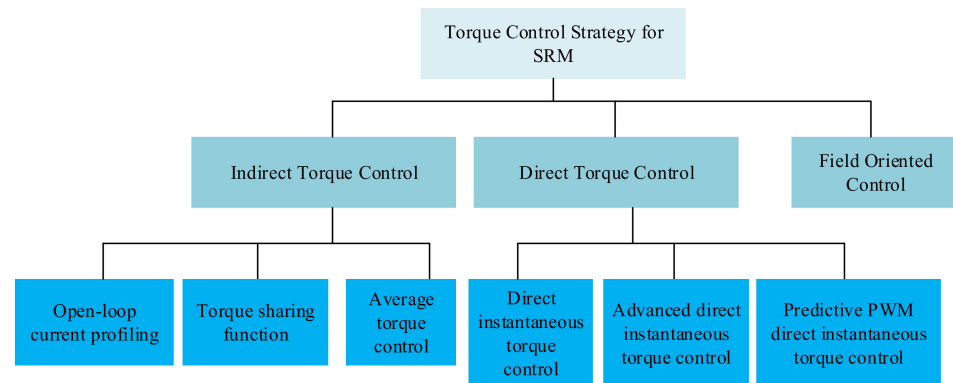


Figure 22. Torque control strategies.

Various kinds of typical control methods are listed and comprehensively compared in Table 4. As listed in Table 4, the open-loop current profiling method establishes lookup tables to calculate the average torque, reference current and switching angle [1,109]. The advantage is the simplicity of calculation. The disadvantage is that it is sensitive to variations due to environmental influences or manufacturing inaccuracies. The TSF method separates reference torque into different phases. Each phase produces torque output individually. It is simpler, more powerful, popular and more efficient. The disadvantage of the TSF is that it needs high bandwidth for the current regulator [110]. The ATC method creates an online average torque estimation to achieve closed-loop control [83–85]. The reference current remains fixed during the excitation. The high torque ripples throughout commutation in the low-speed range is the main disadvantage of the ATC. The DITC method controls the instantaneous torque directly with a hysteresis controller [111,112]. The DITC method can behave as the ADITC method with some PWM techniques [113]. It has an increased switching frequency compared to the DITC. The predictive PWM-DITC predicts the states of the system to optimize the switching state [104]. It has capability to reduce the required bandwidth of the controller. The disadvantage is that the precise information of the machine is needed.

Table 4. Summary and comparison of SRM control strategies.

Control Method	Adopted Technique	Advantage	Disadvantage	Reference
Open-loop current profiling	Offline established lookup tables	Simplicity to calculate average torque.	It is sensitive to variations due to environment influences or production inaccuracies.	[1,109]
Torque sharing function (TSF)	Separated reference torque for different phases	It is simple, powerful, popular and efficient.	A high bandwidth current regulator is needed.	[110]
Average torque control (ATC)	An online average torque estimator	The reference current remains fixed during the excitation.	The torque ripples throughout commutation at the low-speed range.	[105,114,115]
Direct instantaneous torque control (DITC)	Instantaneous controlled torque directly	The set of control variables are simple. The decrease of control variables.	The hysteresis switch rule output one phase state.	[111,112]
Advanced direct instantaneous torque control (ADITC)	A combination of traditional DITC and the PWM	Control the current variety in single sample time.	Switching frequency is increasing compared to DITC.	[113]
Predictive PWM direct instantaneous torque control (PWM-DITC)	Predicted upcoming states	It has ability to reduce the required bandwidth of the controller.	The precise information about the machine characteristics is needed to make reasonable efficiency predictions.	[104]

6. Conclusions and Future Trends

In this paper, the SRM is fully reviewed as a suitable candidate for the EV applications with high torque performance, robust structure and fault tolerance properties. Firstly, the segmental rotor, multi-stack structures, different winding configurations, different drives and control methods are developed to overcome the main drawback of the high torque ripple. When the conventional rotor structure and the segmental rotor structure are compared, the segmental rotor structure has greater torque density under certain conditions. The multi-stack CSRSM and the multi-stack SRM with the segmental rotor are compared and analyzed. The multi-stack structure produces lower torque ripple in standard conditions. Secondly, the single-layer concentrated (SLC), single layer mutually coupled (SLMC), double layer concentrated (DLC), double layer mutually coupled (DLMC), fully-pitched (FP) and toroidal winding SRM (TWSRM) windings are reviewed in this paper. The FP winding with the doubly salient reluctance machine (DSRM) has the highest average torque. Third, the rotor structure has such an important impact on performance. Four types of SRM converters are presented and compared: dissipative, magnetic, resonant and capacitive. It is understood that the capacitive type converter is more effective. In addition, the soft-switching converters for the SRMs are presented. The soft switching reduces the switching losses and voltage stresses of the components. Also, the SRM drive with the standard inverter reduces the cost. For the EV systems, the integrated battery charger with the SRM drive reduces the number of switches required for the vehicle power electronics systems.

Different control methods are assessed in this paper with the ADITC, the DITC, the predicted PWM-DITC, the ATC, the TSC and the current profile control. The predicted PWM-DITC has the best performance because it has fixed switching frequency and has the ability to reduce the bandwidth of the controller. Then, the fault-diagnosis and the fault-tolerance techniques are also reviewed in this paper. These techniques ensure that the SRM keeps operating in a safe way under faulty conditions. Last but not least, the sensorless control method reduces the cost and increases the reliability of the SRM drive system. Thus, segmental rotor, multi-stack, FP winding configuration, predictive PWM-DITC control method and capacitive converter can be considered as preferred approaches for more effective SRM as this combination achieves higher power density and lower torque ripple based on the comparative analysis in this paper. Besides, this review shows higher torque density and lower torque ripple with the segmental rotor and multi-stack configuration. Due to new applications of the segSRMs and the lack of sufficient qualitative papers in the literature about the segmental rotor design for the EV applications, this paper could not cover many utilizations with segSRMs. Finally, the authors tried to provide a useful basis in this paper to define the most proper control schemes, adopted techniques, advantages/disadvantages and design application aspects. In addition, the fundamental design and control principles of the segSRMs have been introduced as a result of a detailed literature survey and this paper aims to provide a reference on the SRMs to readers. The given results in this paper can also be extended with further experimental studies. Furthermore, future research perspectives and forecasted future trends are listed as follows:

- (1) The reduction of the torque ripple should be achieved by developing the multi-stack conventional SRM with less number of switches.
- (2) The torque ripple should be reduced with the multi-stack segSRM with simple topology.
- (3) The drive for the SRMs needs to reach both lower losses and less switches and so should be further developed.
- (4) The control methods to reduce the torque ripple of the SRMs are to be advanced further.
- (5) The fault-diagnosis and the fault-tolerance techniques with simpler and more efficient algorithms should be developed.

Author Contributions: Y.L. reviewed and wrote the first version of the paper; A.A. contributed to reviewing and editing the paper; Y.B. reviewed and improved the editing of the paper; K.D. and M.E.B. reviewed and improved the structure of the paper; E.B. contributed by analyzing and reviewing the paper; O.H. reviewed and edited the manuscript and supervised this research study. All authors have read and agreed to the published version of the manuscript.

Funding: This study was funded by China Scholarship Council (CSC).

Acknowledgments: Yuanfeng Lan was sponsored by China Scholarship Council. The authors also acknowledge Flanders Make for the support to our research group.

Conflicts of Interest: The authors declare no conflict of interest.

Abbreviations

SRM	switched reluctance motor
EV	electric vehicle
MSCSRM	multi-stack conventional switched reluctance motors
MSSRM-SR	multi-stack switched reluctance motors with a segmental rotor
SLC	single-layer concentrated winding
SLMC	single layer mutually coupled winding
DLC	double layer concentrated winding
DLMC	double layer mutually coupled winding
FP	fully-pitched winding
IM	induction motor
PMSM	permanent magnet synchronous motor
VSI	voltage source inverter
CSRM	conventional SRM
EMF	electromotive force
HEV	hybrid EV
AC	alternating current
MIFP	multiple isolated flux
TWSRM	toroidal winding SRM
MMF	magnetomotive force
FEA	finite element analysis
DSRM	doubly salient reluctance machine
UMF	unbalanced magnetic force
SRG	switched reluctance generator
DLPISRM	double-layer-per-phase isolated SRM
DSSRM	double-stator switched reluctance machine
segSRM	segmental SRM
SR	switched reluctance
LOLE	loss of load expectation
PoF	physics of failure
ZVT	zero-voltage transition
AQRDCL	auxiliary quasi-resonant DC-link
IPM	intelligent power module
BLIL	bridgeless interleaved
PV	photovoltaic
MPPT	maximum power point tracking
A + HB	asymmetric bridge and half bridge
NIPC	novel integrated power converter
AHBPC	asymmetric half-bridge power converter
MMC	modular multilevel converter
BESS	battery energy storage system
PFC	power factor correction
DITC	direct instantaneous torque control
ADITC	advanced direct instantaneous torque control

TSF	torque sharing function
FOC	field-oriented control
ARCFL	absolute value of the rate of change of flux linkage
TRFS	torque-ripple-free speed
SPWPS	solar-powered water pumping system
THD	total harmonic distortion
GA	genetic algorithm
SMO	sliding mode observer
ATC	average torque control
DTC	direct torque control
SMO	sliding mode observer

References

- Husain, I. Minimization of torque ripple in SRM drives. *IEEE Trans. Ind. Electron.* **2002**, *49*, 28–39. [CrossRef]
- Beno, M.M.; Marimuthu, N.; Singh, N.A. Improving power factor in switched reluctance motor drive system by optimising the switching angles. In Proceedings of the TENCON 2008 IEEE Region 10 Conference, Hyderabad, India, 19–21 November 2008; pp. 1–5.
- Bostanci, E.; Moallem, M.; Parsapour, A.; Fahimi, B. Opportunities and challenges of switched reluctance motor drives for electric propulsion: A comparative study. *IEEE Trans. Transp. Electrification* **2017**, *3*, 58–75. [CrossRef]
- Gan, C.; Wu, J.; Sun, Q.; Kong, W.; Li, H.; Hu, Y. A review on machine topologies and control techniques for low-noise switched reluctance motors in electric vehicle applications. *IEEE Access* **2018**, *6*, 31430–31443. [CrossRef]
- Torkaman, H.; Afjei, E.; Toulabi, M.S. New double-layer-per-phase isolated switched reluctance motor: Concept, numerical analysis, and experimental confirmation. *IEEE Trans. Ind. Electron.* **2012**, *59*, 830–838. [CrossRef]
- Sun, C.; Zhuang, P.; Li, J.; Li, J. Design and analysis of a 16/6 bearingless switched reluctance motor with segment hybrid rotor teeth. *IEEJ Trans. Electr. Electron. Eng.* **2020**, *15*, 939–946. [CrossRef]
- Polat, M.; Yildiz, A. Influence of different pole head shapes on motor performance in switched reluctance motors. *Adv. Electr. Comput. Eng.* **2020**, *20*, 75–82. [CrossRef]
- Siadatan, A.; Fatahi, N.; Sedaghat, M. Optimum designed multilayer switched reluctance motors for use in electric vehicles to increase efficiency. In Proceedings of the 2018 International Symposium on Power Electronics, Electrical Drives, Automation and Motion (SPEEDAM), Amalfi, Italy, 20–22 June 2018; pp. 304–308.
- Miller, T.J.E. *Switched Reluctance Motors and Their Control*; Magna Physics: Hillsboro, OH, USA; Clarendon Press: Oxford, UK, 1993.
- Gan, C.; Chen, Y.; Qu, R.; Yu, Z.; Kong, W.; Hu, Y. An overview of fault-diagnosis and fault-tolerance techniques for switched reluctance machine systems. *IEEE Access* **2019**, *7*, 174822–174838. [CrossRef]
- Argiolas, O.; Nazeraj, E.; Hegazy, O.; De Backer, J.; Mohammadi, A.; Van Mierlo, J. Design optimization of a 12/8 Switched Reluctance Motor for electric and hybrid vehicles. In Proceedings of the 2017 12th International Conference on Ecological Vehicles and Renewable Energies, EVER 2017, Monte Carlo, Monaco, 11–13 April 2017. [CrossRef]
- Industrail_sr_Brochure. Available online: https://acim.nidec.com/motors/usmotors/-/media/usmotors/documents/literature/brochures/industrial_sr_brochure.ashx (accessed on 20 March 2021).
- Kehui Motor Brochure. Available online: https://www.kehui.com/wp-content/uploads/2018/02/Kehui_motor_brochure.pdf (accessed on 20 March 2021).
- Rocky Mountain Technologies INC. Available online: <http://www.rockymountaintechnologies.com/Standard%20Products.html#> (accessed on 20 March 2021).
- MACCON: Switched Reluctance Motor/Synchronous Reluctance Motor. Available online: <https://www.maccon.com/switched-reluctance-motor-synchronous-reluctance-motor.html> (accessed on 20 March 2021).
- Striatech. Available online: <https://striatech.mybigcommerce.com/> (accessed on 20 March 2021).
- Ma, X.; Li, G.; Zhu, Z.; Jewell, G.W.; Green, J. Investigation on synchronous reluctance machines with different rotor topologies and winding configurations. *IET Electr. Power Appl.* **2018**, *12*, 45–53. [CrossRef]
- Dong, J.; Howey, B.; Danen, B.; Lin, J.; Jiang, J.W.; Bilgin, B.; Emadi, A. Advanced dynamic modeling of three-phase mutually coupled switched reluctance machine. *IEEE Trans. Energy Convers.* **2018**, *33*, 146–154. [CrossRef]
- Azer, P.; Bilgin, B.; Emadi, A. Mutually coupled switched reluctance motor: Fundamentals, control, modeling, state of the art review and future trends. *IEEE Access* **2019**, *7*, 100099–100112. [CrossRef]
- Burruss, T.; Ayers, C. Development and experimental characterization of a Multiple Isolated Flux Path reluctance machine. In Proceedings of the 2012 IEEE Energy Conversion Congress and Exposition (ECCE), Raleigh, NC, USA, 15–20 September 2012.
- Husain, T.; Uddin, W.; Sozer, Y. Performance comparison of short-pitched and fully pitched switched reluctance machines over wide speed operations. *IEEE Trans. Ind. Appl.* **2018**, *54*, 4278–4287. [CrossRef]
- Zuo, S.; Liu, Z.; Hu, S. Influence of rotor eccentricity on radial electromagnetic force characteristics in switched reluctance motors and compensation. *Electr. Power Compon. Syst.* **2020**, *48*, 388–398. [CrossRef]
- Yu, Z.; Gan, C.; Chen, Y.; Qu, R. DC-biased sinusoidal current excited switched reluctance motor drives based on flux modulation principle. *IEEE Trans. Power Electron.* **2020**, *35*, 10614–10628. [CrossRef]

24. Song, S.; Fang, G.; Hei, R.; Jiang, J.; Ma, R.; Liu, W. Torque ripple and efficiency online optimization of switched reluctance machine based on torque per ampere characteristics. *IEEE Trans. Power Electron.* **2020**, *35*, 9608–9616. [[CrossRef](#)]
25. Gan, C.; Chen, Y.; Cui, X.; Sun, J.; Ni, K.; Qu, R. Investigation of rotor strength and rotor dynamics for high-speed high-power switched reluctance machines. *IET Electr. Power Appl.* **2020**, *14*, 1624–1630. [[CrossRef](#)]
26. Diao, K.; Sun, X.; Lei, G.; Guo, Y.; Zhu, J. Multiobjective system level optimization method for switched reluctance motor drive systems using finite-element model. *IEEE Trans. Ind. Electron.* **2020**, *67*, 10055–10064. [[CrossRef](#)]
27. Fan, J.; Lee, Y. Design consideration to achieve wide-speed-range operation in a switched reluctance motor. *Can. J. Electr. Comput. Eng.* **2020**, *43*, 290–294. [[CrossRef](#)]
28. Kucuk, F.; Nakamura, T. Low-cost permanent magnet-assisted switched reluctance motor for adjustable speed drive applications. *IEEJ Trans. Electr. Electron. Eng.* **2020**, *15*, 1213–1218. [[CrossRef](#)]
29. Siadatan, A.; Najmi, V.; Asgar, M.; Afjei, E. A new 6/4 two layers switched reluctance motor: Concept, simulation and analysis. In Proceedings of the International Aegean Conference on Electrical Machines and Power Electronics, ACEMP 2011 and Electromotion 2011 Joint Conference, Istanbul, Turkey, 8 September 2011; pp. 244–249. [[CrossRef](#)]
30. Daldaban, F.; Ustkoyuncu, N. Multi-layer switched reluctance motor to reduce torque ripple. *Energy Convers. Manag.* **2008**, *49*, 974–979. [[CrossRef](#)]
31. Afjei, E.; Torkaman, H.; Mazloomnezhad, B. A new double layer per phase configuration for switched reluctance motor. In Proceedings of the 2010 IEEE International Conference on Power and Energy, Kuala Lumpur, Malaysia, 29 November–1 December 2010; pp. 222–225. [[CrossRef](#)]
32. Siadatan, A.; Najmi, V.; Afjei, E. A novel 4/4 Multilayer Switched Reluctance Motor with 4 magnetically independent layers. In Proceedings of the International Aegean Conference on Electrical Machines and Power Electronics, ACEMP 2011 and Electromotion 2011 Joint Conference, Istanbul, Turkey, 8–10 September 2011; pp. 255–259. [[CrossRef](#)]
33. Afjei, E.; Siadatan, A.; Asgar, M. Comparison between two field-assisted switched reluctance generators suitable for wind turbine applications. In Proceedings of the 2011 International Conference on Clean Electrical Power (ICCEP), Ischia, Italy, 14–16 June 2011; pp. 272–276. [[CrossRef](#)]
34. Najmi, V.; Siadatan, A.; Asgar, M.; Afjei, E. Magnetostatic analysis of a novel three phase 6/4 two layer field-assisted Switched Reluctance Generator. In Proceedings of the International Aegean Conference on Electrical Machines and Power Electronics, ACEMP 2011 and Electromotion 2011 Joint Conference, Istanbul, Turkey, 8–10 September 2011; pp. 266–269. [[CrossRef](#)]
35. Jahanmahin, M.; Hajihosseini, A.; Afjei, E.; Siadatan, A.; Tavakoli, A. A novel multilayer 8 by 4 switch reluctance machine with ripple reduction. In Proceedings of the International Symposium on Power Electronics Power Electronics, Electrical Drives, Automation and Motion, Virtual, Sorrento, Italy, 24–26 June 2020; pp. 536–540.
36. Najmi, V.; Siadatan, A.; Afjei, E. Analysis of 8/6 two-layer switched reluctance motor with rotor shifting technique for servo applications. In Proceedings of the 2012 3rd Power Electronics and Drive Systems Technology, PEDSTC 2012, Tehran, Iran, 15–16 February 2012; pp. 273–277. [[CrossRef](#)]
37. Salimi, A.; Rezazadeh, G.; Nourollah, S.; Niassati, N.; Hajihosseini, A. A novel four layer switch reluctance generator. In Proceedings of the 2012 15th International Power Electronics and Motion Control Conference (EPE/PEMC), Novi Sad, Serbia, 4–6 September 2012; p. LS1b.2-1.
38. Hajihosseini, A.; Jahanmahin, M.; Afjei, E.; Tajik, S. A novel four layer switch reluctance motor with high torque and ripple reduction. In Proceedings of the 2012 3rd Power Electronics and Drive Systems Technology, PEDSTC 2012, Tehran, Iran, 15–16 February 2012; pp. 62–67. [[CrossRef](#)]
39. Siadatan, A.; Rafiee, M.; Afjei, E. Design, analysis and controlling of a novel 4 by 4 multilayer SRM. In Proceedings of the 2013 21st Iranian Conference on Electrical Engineering (ICEE), Mashhad, Iran, 14–16 May 2013; pp. 1–5. [[CrossRef](#)]
40. Siadatan, A.; Afjei, E.; Torkaman, H.; Rafie, M. Design, simulation and experimental results for a novel type of two-layer 6/4 three-phase switched reluctance motor/generator. *Energy Convers. Manag.* **2013**, *71*, 199–207. [[CrossRef](#)]
41. Sugiura, M.; Ishihara, Y.; Ishikawa, H.; Naitoh, H. Improvement of efficiency by stepped-skewing rotor for switched reluctance motors. In Proceedings of the 2014 International Power Electronics Conference (IPEC-Hiroshima 2014—ECCE ASIA), Hiroshima, Japan, 18–21 May 2014; pp. 1135–1140. [[CrossRef](#)]
42. Siadatan, A.; Afjei, E.; Mahmoodi, M.M. Torque comparison between a novel Multilayer Switched Reluctance Motor and a custom one. In Proceedings of the 2014 International Symposium on Power Electronics, Electrical Drives, Automation and Motion, Ischia, Italy, 18–20 June 2014; pp. 409–416. [[CrossRef](#)]
43. Siadatan, A.; Torkaman, H.; Afjei, E. Septi-segment switched reluctance machine: Design, modeling, and manufacturing. *Int. Trans. Electr. Energy Syst.* **2016**, *26*, 1673–1684. [[CrossRef](#)]
44. Gu, L.; Wang, W.; Fahimi, B.; Clark, A.; Hearn, J. Magnetic design of two-phase switched reluctance motor with bidirectional startup capability. *IEEE Trans. Ind. Appl.* **2016**, *52*, 2148–2155. [[CrossRef](#)]
45. Hekmati, P.; Brown, I.P. Rotary-reciprocating movement switched-reluctance machines with consequent axially shifted poles. *IEEE Trans. Magn.* **2018**, *54*, 1–10. [[CrossRef](#)]
46. Siadatan, A.; Najmi, V.; Afjei, E. Modeling, simulation and analysis of a novel two layer 8/6 hybrid switched reluctance motor/field-assisted generator. In Proceedings of the 2012 20th Iranian Conference on Electrical Engineering (ICEE2012), Tehran, Iran, 15–17 May 2012; IEEE, 2012; pp. 495–500. [[CrossRef](#)]

47. Kondelaji, M.A.J.; Mirsalim, M. Non-linear modeling of a multi-layer switched reluctance motor with magnetically-disconnected stator modules. In Proceedings of the 2019 10th International Power Electronics, Drive Systems and Technologies Conference (PEDSTC), Shiraz, Iran, 12–14 February 2019; pp. 1–6. [\[CrossRef\]](#)
48. Vahedi, P.; Ganji, B.; Afjei, E. Multi-layer switched reluctance motors: Performance prediction and torque ripple reduction. *Int. Trans. Electr. Energy Syst.* **2019**, *30*. [\[CrossRef\]](#)
49. Luk, P.C.K.; Jinupun, K.P. Direct work control for a three-stack switched reluctance motor. In Proceedings of the 2005 IEEE 36th Power Electronics Specialists Conference, Recife, Brazil, 12–16 June 2005; IEEE, 2006; pp. 2462–2466.
50. Vatani, M.; Mirsalim, M.; Vaez-Zadeh, S. A New double-layer switched reluctance motor with a low torque ripple. In Proceedings of the 2019 27th Iranian Conference on Electrical Engineering (ICEE), Yazd, Iran, 30 April–2 May 2019; pp. 792–797.
51. Mecrow, B.; Finch, J.; El-Kharashi, E.; Jack, A. Switched reluctance motors with segmental rotors. *IEE Proc. Electr. Power Appl.* **2002**, *149*, 245. [\[CrossRef\]](#)
52. Mecrow, B.; El-Kharashi, E.; Finch, J.; Jack, A. Segmental rotor switched reluctance motors with single-tooth windings. *IEE Proc. Electr. Power Appl.* **2003**, *150*, 591. [\[CrossRef\]](#)
53. Abbasian, M.; Moallem, M.; Fahimi, B. Double-Stator Switched Reluctance Machines (DSSRM): Fundamentals and magnetic force analysis. *IEEE Trans. Energy Convers.* **2010**, *25*, 589–597. [\[CrossRef\]](#)
54. Bostanci, E.; Gu, L.; Cosoroaba, E.; Moallem, M.; Fahimi, B. Performance improvement and comparison of concentrated winding segmental rotor and double stator switched reluctance machines. In Proceedings of the 2016 IEEE Conference on Electromagnetic Field Computation (CEFC), Miami, FL, USA, 13–16 November 2016; p. 1.
55. Oyama, J.; Higuchi, T.; Abe, T.; Kifuji, N. Novel switched reluctance motor with segment core embedded in aluminum rotor block. *IEEJ Trans. Ind. Appl.* **2006**, *126*, 385–390. [\[CrossRef\]](#)
56. Deng, X.; Mecrow, B. A comparison of conventional and segmental rotor 12/10 switched reluctance motors. In Proceedings of the 2019 IEEE International Electric Machines and Drives Conference, IEMDC 2019, San Diego, CA, USA, 12–15 May 2019; pp. 1508–1513. [\[CrossRef\]](#)
57. Chen, L.; Wang, H.; Sun, X.; Cai, Y.; Li, K.; Diao, K.; Wu, J. Development of a digital control system for a belt-driven starter generator segmented switched reluctance motor for hybrid electric vehicles. *Proc. Inst. Mech. Eng. Part I J. Syst. Control Eng.* **2020**, *234*, 975–984. [\[CrossRef\]](#)
58. Abdollahi, M.; Mirsalim, M. Novel E-Core Double-Stator Two Phase Switched Reluctance Motor with Segmental Rotor. In Proceedings of the 2019 10th International Power Electronics, Drive Systems and Technologies Conference (PEDSTC), Shiraz, Iran, 12–14 February 2019; pp. 72–77. [\[CrossRef\]](#)
59. Higuchi, T.; Ueda, T.; Abe, T. Torque ripple reduction control of a novel segment type SRM with 2-steps slide rotor. In Proceedings of the 2010 International Power Electronics Conference—ECCE ASIA, Sapporo, Japan, 21–24 June 2010; pp. 2175–2180. [\[CrossRef\]](#)
60. Higuchi, T.; Nakao, Y.; Abe, T. Characteristics of a novel segment type SRM with 2-step slide rotor. In Proceedings of the 2009 International Conference on Electrical Machines and Systems, Tokyo, Japan, 15–18 November 2009; pp. 1–4. [\[CrossRef\]](#)
61. Lan, Y.; Peng, W.; Aksoz, A.; Benomar, Y.; Bossche, P.V.D.; El, M.; Hegazy, O. Design and Modelling of 12/4 Fully-Pitched Segmental Switched Reluctance Motors. In Proceedings of the 2020 Fifteenth International Conference on Ecological Vehicles and Renewable Energies (EVER), Monte-Carlo, Monaco, 10–12 September 2020.
62. Mecrow, B.; El-Kharashi, E.; Finch, J.; Jack, A. Preliminary performance evaluation of switched reluctance motors with segmental rotors. *IEEE Trans. Energy Convers.* **2004**, *19*, 679–686. [\[CrossRef\]](#)
63. Mukhopadhyay, J.; Sengupta, S.; Choudhuri, S. Drive strategies for switched reluctance motor—A review. In Proceedings of the Michael Faraday IET International Summit 2015, Kolkata, India, 12–13 September 2015; Volume 23. [\[CrossRef\]](#)
64. Ahn, J.-W.; Liang, J.; Lee, D.-H. Classification and analysis of switched reluctance converters. *J. Electr. Eng. Technol.* **2010**, *5*, 571–579. [\[CrossRef\]](#)
65. Krishnan, R. Switched reluctance motor drives. In Proceedings of the Industrial Electronics 2017, Siem Reap, Cambodia, 18–20 June 2017.
66. Pittermann, M.; Fort, J.; Diesl, J.; Pavlicek, V. Converters for Switched Reluctance Motor—Topology Comparison. In Proceedings of the 2018 18th International Conference on Mechatronics—Mechatronika, ME, Brno, Czech Republic, 5–7 December 2018; pp. 1–8.
67. Peyghami, S.; Davari, P.; Wang, H.; Blaabjerg, F. Reliability and risk assessment in a Power Electronic Based Power System (PEPS): Using non-constant failure rates of converters. In Proceedings of the 2018 20th European Conference on Power Electronics and Applications, EPE 2018 ECCE Europe, Riga, Latvia, 17–21 September 2018.
68. Maier, R.W.; Bakran, M.M. Switching SiC MOSFETs under conditions of a high power module. In Proceedings of the 2018 20th European Conference on Power Electronics and Applications, EPE 2018 ECCE Europe, Riga, Latvia, 17–21 September 2018; p. 2.
69. Kiani, E.; Ganji, B.; Taher, S.A. Model predictive control of switched reluctance generator based on Z-source converter for wind power applications. *Int. Trans. Electr. Energy Syst.* **2020**, *30*, e12578. [\[CrossRef\]](#)
70. Jing, J. A Power factor correction buck converter-fed switched reluctance motor with torque ripple suppression. *Math. Probl. Eng.* **2020**, *2020*, 6730284. [\[CrossRef\]](#)
71. Chaple, M.D.; Bodkhe, S.B. An integrated converter model and enhanced control approach for torque ripple minimisation of switched reluctance motor: A CMFG-RNN technique. *Int. J. Ambient. Energy* **2018**, *41*, 1142–1153. [\[CrossRef\]](#)

72. Ellabban, O.; Abu-Rub, H. Switched reluctance motor converter topologies: A review. In Proceedings of the 2014 IEEE International Conference on Industrial Technology (ICIT), Busan, Korea, 26 February–1 March 2014; pp. 840–846. [[CrossRef](#)]
73. Kabir, A.; Husain, I. Hybrid excitation topologies for three-phase mutually coupled reluctance machine with standard inverters. In Proceedings of the 2015 IEEE Power & Energy Society General Meeting, Denver, CO, USA, 26–30 July 2015; pp. 1–5. [[CrossRef](#)]
74. Kabir, M.A.; Husain, I. Concentrated winding segmented rotor switched reluctance machine (SRM) using three-phase standard inverters. In Proceedings of the 2015 IEEE Energy Conversion Congress and Exposition, ECCE 2015, Montreal, QC, Canada, 20–24 September 2015; pp. 5567–5572. [[CrossRef](#)]
75. Kabir, A.; Husain, I. Design of Mutually Coupled Switched Reluctance Motors (MCSRMs) for extended speed applications using 3-phase standard inverters. *IEEE Trans. Energy Convers.* **2016**, *31*, 436–445. [[CrossRef](#)]
76. Chen, Q.; Xu, D.; Xu, L.; Wang, J.; Lin, Z.; Zhu, X. Fault-tolerant operation of a novel dual-channel switched reluctance motor using two 3-phase standard inverters. *IEEE Trans. Appl. Supercond.* **2018**, *28*, 1–5. [[CrossRef](#)]
77. Subotic, I.; Levi, E. A review of single-phase on-board integrated battery charging topologies for electric vehicles. In Proceedings of the 2015 IEEE Workshop on Electrical Machines Design, Control and Diagnosis (WEMDCD), Torino, Italy, 26–27 March 2015; pp. 136–145. [[CrossRef](#)]
78. Na, T.; Yuan, X.; Tang, J.; Zhang, Q. A Review of on-board integrated charger for electric vehicles and a new solution. In Proceedings of the 2019 IEEE 10th International Symposium on Power Electronics for Distributed Generation Systems (PEDG), Xi'an, China, 3–6 June 2019; pp. 693–699.
79. Drive, M.; Power, U.T.-P.; Chang, H.-C.; Liaw, C.-M. An Integrated Driving/Charging Switched Reluctance motor drive using three-phase power module. *IEEE Trans. Ind. Electron.* **2011**, *58*, 1763–1775.
80. Huseini, S.R.K.; Farjah, E.; Tashakor, N.; Ghanbari, T. Development of an integrated Switched-Reluctance Motor drive with battery charging capability for electric vehicle propulsion system. In Proceedings of the 6th Power Electronics, Drive Systems & Technologies Conference (PEDSTC2015), Tehran, Iran, 3–4 February 2015; pp. 579–584. [[CrossRef](#)]
81. Jiang, J.; Xia, T. An integrated charger with central-tapped winding switched reluctance motor drive. In Proceedings of the 2017 IEEE 6th International Conference on Renewable Energy Research and Applications (ICRERA), San Diego, CA, USA, 5–8 November 2017; pp. 870–874.
82. Liang, J.; Li, W.; Song, Z.; Shi, Y. An integrated battery charger base on split-winding switched reluctance motor drive. In Proceedings of the 2016 IEEE Transportation Electrification Conference and Expo, Asia-Pacific (ITEC Asia-Pacific), Busan, Korea, 1–4 June 2016; pp. 106–111.
83. Deriszadeh, A.; Bojoi, R. An integrated battery-charger for switched reluctance motor drives. In Proceedings of the 2017 6th International Conference on Clean Electrical Power (ICCEP), Liguria, Italy, 27–29 June 2017; pp. 446–451. [[CrossRef](#)]
84. Liang, J.; Sun, T. Design of Integrated Battery Charger Based on Switched Reluctance Motor Drive. In Proceedings of the 2018 21st International Conference on Electrical Machines and Systems (ICEMS), Jeju, Korea, 7–10 October 2018.
85. Feng, C.; Wu, J.; Sun, Q.; Wu, H.; Zhang, L. An Integrated BLIL Boost Converter-based Switched Reluctance Motor Drive for PEV Applications with PFC Charging Function. In Proceedings of the 2019 22nd International Conference on Electrical Machines and Systems (ICEMS), Harbin, China, 11–14 August 2019; p. 4. [[CrossRef](#)]
86. Saeed, J.; Niakinezhad, M.; Wang, L.; Fetnando, N. An Integrated Charger with Hybrid Power Source Using PV Array for EV Application. In Proceedings of the 2019 IEEE 13th International Conference on Compatibility, Power Electronics and Power Engineering (CPE-POWERENG), Sonderborg, Denmark, 23–25 April 2019; pp. 1–6.
87. Reimers, J.; Emadi, A. Switched Reluctance Motor Drive with Three-Phase Integrated Battery Charger for Electric Vehicle Applications. In Proceedings of the 2019 IEEE 28th International Symposium on Industrial Electronics (ISIE), Vancouver, BC, Canada, 12–14 June 2019; pp. 2097–2102. [[CrossRef](#)]
88. Xu, S.; Chen, H.; Yang, J.; Dong, F. Performance evaluation and reliability enhancement of switched reluctance drive system by a novel integrated power converter. *IEEE Trans. Power Electron.* **2019**, *34*, 11090–11102. [[CrossRef](#)]
89. Chen, H.-C.; Wang, W.-A.; Huang, B.-W. Integrated driving/charging/discharging battery-powered four-phase switched reluctance motor drive with two current sensors. *IEEE Trans. Power Electron.* **2018**, *34*, 5019–5022. [[CrossRef](#)]
90. Gan, C.; Sun, Q.; Wu, J.; Kong, W.; Shi, C.; Hu, Y. MMC-based SRM drives with decentralized battery energy storage system for hybrid electric vehicles. *IEEE Trans. Power Electron.* **2019**, *34*, 2608–2621. [[CrossRef](#)]
91. Cheng, H.; Wang, Z.; Yang, S.; Huang, J.; Ge, X. An integrated SRM powertrain topology for plug-in hybrid electric vehicles with multiple driving and onboard charging capabilities. *IEEE Trans. Transp. Electrif.* **2020**, *6*, 578–591. [[CrossRef](#)]
92. Cai, J.; Zhao, X. An on-board charger integrated power converter for EV switched reluctance motor drives. *IEEE Trans. Ind. Electron.* **2021**, *68*, 3683–3692. [[CrossRef](#)]
93. Cheng, H.; Wang, L.; Xu, L.; Ge, X.; Yang, S. An integrated electrified powertrain topology with SRG and SRM for plug-in hybrid electrical vehicle. *IEEE Trans. Ind. Electron.* **2019**, *67*, 8231–8241. [[CrossRef](#)]
94. Ghani, M.R.A.; Farah, N.; Tamjis, M.R. Field oriented control of 6/4 SRM for torque ripple minimization. In Proceedings of the International Conference on Electrical, Electronics, and Optimization Techniques, ICEEOT, Chennai, India, 3–5 March 2016; pp. 4418–4424. [[CrossRef](#)]
95. Mishra, A.K.; Singh, B. An efficient control scheme of grid supported 4-phase switched reluctance motor-driven SPWPS. *IEEE Trans. Energy Convers.* **2020**, *35*, 1258–1267. [[CrossRef](#)]

96. Üstün, O.; Önder, M. An improved torque sharing function to minimize torque ripple and increase average torque for switched reluctance motor drives. *Electr. Power Compon. Syst.* **2020**, *48*, 667–681. [[CrossRef](#)]
97. Li, S.; Moallem, M.; Balsara, P.T.; Fahimi, B. Chaos in the switched reluctance motor drive employing digital speed and current control. *IET Power Electron.* **2020**, *13*, 1656–1666. [[CrossRef](#)]
98. Jamil, M.U.; Kongprawechnon, W.; Chayopitak, N. Active fault diagnosis of a switched reluctance motor using sliding mode observer and average torque estimator for light electric vehicle applications. *Int. Trans. Electr. Energy Syst.* **2020**, *30*, e12602. [[CrossRef](#)]
99. Huang, L.; Zhu, Z.Q.; Feng, J.; Guo, S.; Li, Y.; Shi, J.X. Novel current profile of switched reluctance machines for torque density enhancement in low-speed applications. *IEEE Trans. Ind. Electron.* **2019**, *67*, 9623–9634. [[CrossRef](#)]
100. Dang, X.; Shi, Y.; Peng, H. Torque–flux linkage recurrent neural network adaptive inversion control of torque for switched reluctance motor. *IET Electr. Power Appl.* **2020**, *14*, 1612–1623. [[CrossRef](#)]
101. Ben Salem, F.; Bahri, I.; Maamri, H.; Derbel, N. A second-order sliding mode control of switched reluctance motor. *Electr. Power Compon. Syst.* **2020**, *48*, 1–12. [[CrossRef](#)]
102. Anuchin, A.; Demidova, G.L.; Hao, C.; Zharkov, A.; Bogdanov, A.; Šmídl, V. Continuous control set model predictive control of a switch reluctance drive using lookup tables. *Energies* **2020**, *13*, 3317. [[CrossRef](#)]
103. Fan, J.; Lee, Y. A Novel average torque control of switched reluctance motor based on flux–current locus control. *Can. J. Electr. Comput. Eng.* **2020**, *43*, 273–281. [[CrossRef](#)]
104. Brauer, H.J.; Hennen, M.D.; De Doncker, R.W. Multiphase torque-sharing concepts of predictive PWM-DITC for SRM. In Proceedings of the 2007 7th International Conference on Power Electronics and Drive Systems, Bangkok, Thailand, 27–30 November 2007; pp. 511–516.
105. Cheng, H.; Chen, H.; Yang, Z. Average torque control of switched reluctance machine drives for electric vehicles. *IET Electr. Power Appl.* **2015**, *9*, 459–468. [[CrossRef](#)]
106. Wang, D.; Zhang, D.; Du, X.; Wang, X. Thermal identification, model, and experimental validation of a toroidally wound mover linear-switched reluctance machine. *IEEE Trans. Magn.* **2017**, *54*, 1–5. [[CrossRef](#)]
107. Gan, C.; Sun, Q.; Wu, J.; Shi, C.; Hu, Y. A universal two-sensor current detection scheme for current control of multiphase switched reluctance motors with multiphase excitation. *IEEE Trans. Power Electron.* **2018**, *34*, 1526–1539. [[CrossRef](#)]
108. Abdel-Fadil, R.; Szamel, L. State of the art of switched reluctance motor drives and control techniques. In Proceedings of the 2018 Twentieth International Middle East Power Systems Conference (MEPCON), Cairo, Egypt, 18–20 December 2018; pp. 779–784.
109. Inderka, R.; Menne, M.; De Doncker, R. Control of switched reluctance drives for electric vehicle applications. *IEEE Trans. Ind. Electron.* **2002**, *49*, 48–53. [[CrossRef](#)]
110. Evangeline, S.; Kumar, S. Torque ripple minimization of switched reluctance drives—A survey. In Proceedings of the 5th IET International Conference on Power Electronics, Machines and Drives (PEMD 2010), Brighton, UK, 19–21 April 2010.
111. Inderka, R.; De Doncker, R. DITC-direct instantaneous torque control of switched reluctance drives. *IEEE Trans. Ind. Appl.* **2003**, *39*, 1046–1051. [[CrossRef](#)]
112. Fuengwarodsakul, N.; Menne, M.; Inderka, R.; De Doncker, R. High-dynamic four-quadrant switched reluctance drive based on DITC. *IEEE Trans. Ind. Appl.* **2005**, *41*, 1232–1242. [[CrossRef](#)]
113. Neuhaus, C.; Fuengwarodsakul, N.; De Doncker, R. Predictive PWM-based direct instantaneous torque control of switched reluctance drives. In Proceedings of the 37th IEEE Power Electronics Specialists Conference, Jeju, Korea, 8–22 June 2006; pp. 1–7.
114. Inderka, R.; De Doncker, R. High-dynamic direct average torque control for switched reluctance drives. *IEEE Trans. Ind. Appl.* **2003**, *39*, 1040–1045. [[CrossRef](#)]
115. Hannoun, H.; Hilairret, M.; Marchand, C. Design of an SRM speed control strategy for a wide range of operating speeds. *IEEE Trans. Ind. Electron.* **2010**, *57*, 2911–2921. [[CrossRef](#)]